

---

# Self-Supervised Learning with Kernel Dependence Maximization

---

**Yazhe Li\***

DeepMind and Gatsby Unit, UCL  
yazhe@google.com

**Roman Pogodin\***

Gatsby Unit, UCL  
roman.pogodin.17@ucl.ac.uk

**Danica J. Sutherland**

UBC and Amii<sup>†</sup>  
dsuth@cs.ubc.ca

**Arthur Gretton**

Gatsby Unit, UCL  
arthur.gretton@gmail.com

## Abstract

We approach self-supervised learning of image representations from a statistical dependence perspective, proposing Self-Supervised Learning with the Hilbert-Schmidt Independence Criterion (SSL-HSIC). SSL-HSIC maximizes dependence between representations of transformations of an image and the image identity, while minimizing the kernelized variance of those representations. This framework yields a new understanding of InfoNCE, a variational lower bound on the mutual information (MI) between different transformations. While the MI itself is known to have pathologies which can result in learning meaningless representations, its bound is much better behaved: we show that it implicitly approximates SSL-HSIC (with a slightly different regularizer). Our approach also gives us insight into BYOL, a negative-free SSL method, since SSL-HSIC similarly learns local neighborhoods of samples. SSL-HSIC allows us to directly optimize statistical dependence in time linear in the batch size, without restrictive data assumptions or indirect mutual information estimators. Trained with or without a target network, SSL-HSIC matches the current state-of-the-art for standard linear evaluation on ImageNet [1], semi-supervised learning and transfer to other classification and vision tasks such as semantic segmentation, depth estimation and object recognition. Code is available at [https://github.com/deepmind/ssl\\_hsic](https://github.com/deepmind/ssl_hsic).

## 1 Introduction

Learning general-purpose visual representations without human supervision is a long-standing goal of machine learning. Specifically, we wish to find a feature extractor that captures the image semantics of a large unlabeled collection of images, so that e.g. various image understanding tasks can be achieved with simple linear models. One approach takes the latent representation of a likelihood-based generative model [2–8]; such models, though, solve a harder problem than necessary since semantic features need not capture low-level details of the input. Another option is to train a *self-supervised* model for a “pretext task,” such as predicting the position of image patches, identifying rotations, or image inpainting [9–14]. Designing good pretext tasks, however, is a subtle art, with little theoretical guidance available. Recently, a class of models based on contrastive learning [15–22] has seen substantial success: dataset images are cropped, rotated, color shifted, etc. into several *views*, and features are then trained to pull together representations of the “positive” pairs of views of the same

---

\*These authors contributed equally.

<sup>†</sup>Work done in part while at the Toyota Technological Institute at Chicago.

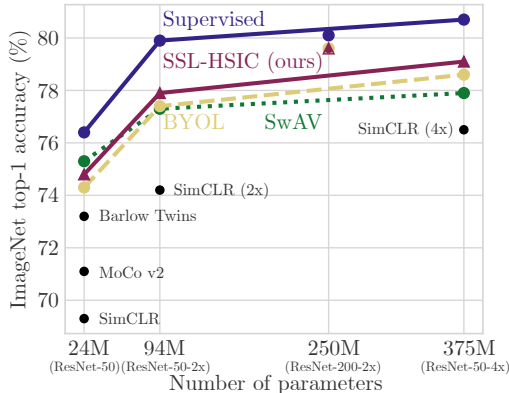


Figure 1: Top-1 accuracies with linear evaluation for different ResNet architecture and methods: supervised (as in [25]), SSL-HSIC (with a target network; ours), BYOL [25], SwAV [18], SimCLR [19], MoCo v2 [20] and Barlow Twins [22].

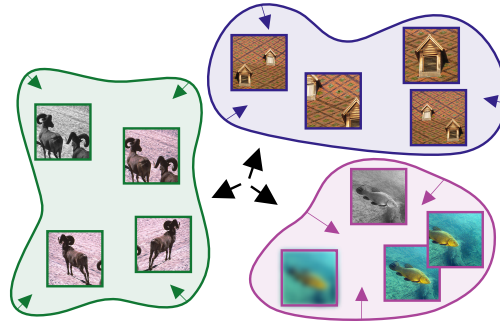


Figure 2: Statistical dependence view of contrastive learning: representations of transformed images should highly depend on image identity. Measuring dependence with HSIC, this pushes different images’ representation distributions apart (black arrows) and pulls representations of the same image together (colored shapes).

source image, and push apart those of “negative” pairs (from different images). These methods are either understood from an information theoretic perspective as estimating the mutual information between the “positives” [15], or explained as aligning features subject to a uniformity constraint [23]. Another line of research [24, 25] attempts to learn representation without the “negative” pairs, but requires either a target network or stop-gradient operation to avoid collapsing.

We examine the contrastive framework from a statistical dependence point of view: feature representations for a given transformed image should be highly dependent on the image identity (Figure 2). To measure dependence, we turn to the Hilbert-Schmidt Independence Criterion (HSIC) [26], and propose a new loss for self-supervised learning which we call SSL-HSIC. Our loss is inspired by HSIC Bottleneck [27, 28], an alternative to Information Bottleneck [29], where we use the image identity as the label, but change the regularization term.

Through the dependence maximization perspective, we present a unified view of various self-supervised losses. Previous work [30] has shown that the success of InfoNCE cannot be solely attributed to properties of mutual information, in particular because mutual information (unlike kernel measures of dependence) has no notion of geometry in feature space: for instance, *all* invertible encoders achieve maximal mutual information, but they can output dramatically different representations with very different downstream performance [30]. Variational bounds on mutual information do impart notions of locality that allow them to succeed in practice, departing from the mutual information quantity that they try to estimate. We prove that InfoNCE, a popular such bound, in fact approximates SSL-HSIC with a variance-based regularization. Thus, InfoNCE can be thought of as working because it implicitly estimates a kernel-based notion of dependence. We additionally show SSL-HSIC is related to metric learning, where the features learn to align to the structure induced by the self-supervised labels. This perspective is closely related to the objective of BYOL [25], and can explain properties such as alignment and uniformity [23] observed in contrastive learning.

Our perspective brings additional advantages, in computation and in simplicity of the algorithm, compared with existing approaches. Unlike the indirect variational bounds on mutual information [15, 31, 32], SSL-HSIC can be directly estimated from mini-batches of data. Unlike “negative-free” methods, the SSL-HSIC loss itself penalizes trivial solutions, so techniques such as target networks are not needed for reasonable outcomes. Using a target network does improve the performance of our method, however, suggesting target networks have other advantages that are not yet well understood. Finally, we employ random Fourier features [33] in our implementation, resulting in cost linear in batch size.

Our main contributions are as follows:

- We introduce SSL-HSIC, a principled self-supervised loss using kernel dependence maximization.
- We present a unified view of contrastive learning through dependence maximization, by establishing relationships between SSL-HSIC, InfoNCE, and metric learning.

- Our method achieves top-1 accuracy of 74.8% and top-5 accuracy of 92.2% with linear evaluations (see Figure 1 for a comparison with other methods), top-1 accuracy of 80.2% and Top-5 accuracy of 94.7% with fine-tuning, and competitive performance on a diverse set of downstream tasks.

## 2 Background

### 2.1 Self-supervised learning

Recent developments in self-supervised learning, such as contrastive learning, try to ensure that features of two random views of an image are more associated with each other than with random views of other images. Typically, this is done through some variant of a classification loss, with one “positive” pair and many “negatives.” Other methods can learn solely from “positive” pairs, however. There have been many variations of this general framework in the past few years.

Van den Oord et al. [15] first formulated the InfoNCE loss, which estimates a lower bound of the mutual information between the feature and the context. SimCLR [19, 34] carefully investigates the contribution of different data augmentations, and scales up the training batch size to include more negative examples. MoCo [17] increases the number of negative examples by using a memory bank. BYOL [25] learns solely on positive image pairs, training so that representations of one view match that of the other under a moving average of the featurizer. Instead of the moving average, SimSiam [24] suggests a stop-gradient on one of the encoders is enough to prevent BYOL from finding trivial solutions. SwAV [18] clusters the representation online, and uses distance from the cluster centers rather than computing pairwise distances of the data. Barlow Twins [22] uses an objective related to the cross-correlation matrix of the two views, motivated by redundancy reduction. It is perhaps the most related to our work in the literature (and their covariance matrix can be connected to HSIC [35]), but our method measures dependency more directly. While Barlow Twins decorrelates components of final representations, we maximize the dependence between the image’s abstract identity and its transformations.

On the theory side, InfoNCE is proposed as a variational bound on Mutual Information between the representation of two views of the same image [15, 32]. Tschannen et al. [30] observe that InfoNCE performance cannot be explained solely by the properties of the mutual information, however, but is influenced more by other factors, such as the formulation of the estimator and the architecture of the feature extractor. Essentially, representations with the same MI can have drastically different representational qualities. To see this, consider a problem with two inputs,  $A$  and  $B$  (Figure 3, green and purple), and a one-dimensional featurizer, parameterized by the integer  $M$ , which maps  $A$  to  $\text{Uniform}(\{0, 2, \dots, 2M\})$  and  $B$  to  $\text{Uniform}(\{1, 3, \dots, 2M + 1\})$ . When  $M = 0$ , the inputs are encoded into linearly separable features  $A = 0$  and  $B = 1$  (Figure 3, bottom). Otherwise when  $M > 0$ , they are interspersed like  $ABABABAB$  – a representation which is much harder to work with for downstream learners. Nevertheless, the mutual information between the features of any two augmentations of the same input (a positive pair) is independent of  $M$ , that is  $H[Z_1] - H[Z_1|Z_2] = \log 2$  for any  $M$ . Note that InfoNCE would strongly prefer  $M = 0$ , indeed behaving very differently from MI.

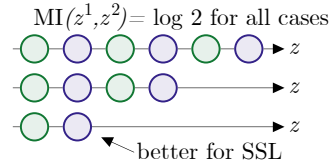


Figure 3: Three distributions of positive examples for two classes (green and purple) that have the same mutual information, but drastically different quality for downstream learners.

Later theories suggest that contrastive losses balance alignment of individual features and uniformity of the feature distribution [23], or in general alignment and some loss-defined distribution [36]. We propose to interpret the contrastive loss through the lens of statistical dependence, and relate it to metric learning, which naturally leads to alignment and uniformity.

### 2.2 Hilbert-Schmidt Independence Criterion (HSIC)

The Hilbert-Schmidt Independence Criterion (HSIC) [26] is a kernel-based measure of dependence between probability distributions. Like mutual information, for a wide range of kernels  $\text{HSIC}(X, Y) = 0$  if and only if  $X$  and  $Y$  are independent [37], and large values of the measure correspond to “more dependence.” Unlike mutual information, HSIC incorporates a notion of ge-

ometry (via the kernel choice), and is both statistically and computationally easy to estimate. It has been used in a variety of applications, particularly for independence testing [38], but it has also been maximized in applications such as feature selection [39], clustering [40, 41], active learning [42], and as a classification loss called HSIC Bottleneck [27, 28] (similar ideas were expressed in [43, 44]).

HSIC measures the dependence between two random variables by first taking a nonlinear feature transformation of each, say  $\phi : \mathcal{X} \rightarrow \mathcal{F}$  and  $\psi : \mathcal{Y} \rightarrow \mathcal{G}$  (with  $\mathcal{F}$  and  $\mathcal{G}$  reproducing kernel Hilbert spaces, RKHSes<sup>1</sup>), and then evaluating the norm of the cross-covariance between those features:

$$\text{HSIC}(X, Y) = \|\mathbb{E}[\phi(X) \psi(Y)^\top] - \mathbb{E}[\phi(X)] \mathbb{E}[\psi(Y)]^\top\|_{HS}^2. \quad (1)$$

Here  $\|\cdot\|_{HS}$  is the Hilbert-Schmidt norm, which in finite dimensions is the usual Frobenius norm. HSIC measures the scale of the correlation in these nonlinear features, which allows it to identify nonlinear dependencies between  $X$  and  $Y$  with appropriate features  $\phi$  and  $\psi$ .

Inner products in an RKHS are by definition *kernel functions*:  $k(x, x') = \langle \phi(x), \phi(x') \rangle_{\mathcal{F}}$  and  $l(y, y') = \langle \psi(y), \psi(y') \rangle_{\mathcal{G}}$ . Let  $(X', Y')$ ,  $(X'', Y'')$  be independent copies of  $(X, Y)$ ; this gives

$$\text{HSIC}(X, Y) = \mathbb{E}[k(X, X')l(Y, Y')] - 2\mathbb{E}[k(X, X')l(Y, Y'')] + \mathbb{E}[k(X, X')] \mathbb{E}[l(Y, Y')]. \quad (2)$$

HSIC is also straightforward to estimate: given i.i.d. samples  $\{(x_1, y_1), \dots, (x_N, y_N)\}$  drawn i.i.d. from the joint distribution of  $(X, Y)$ , Gretton et al. [26] propose an estimator

$$\widehat{\text{HSIC}}(X, Y) = \frac{1}{(N-1)^2} \text{Tr}(KHLH), \quad (3)$$

where  $K_{ij} = k(x_i, x_j)$  and  $L_{ij} = l(y_i, y_j)$  are the kernel matrices, and  $H = I - \frac{1}{N}\mathbf{1}\mathbf{1}^\top$  is called the centering matrix. This estimator has an  $O(1/N)$  bias, which is not a concern for our uses; however, an unbiased estimator with the same computational cost is available [39].

### 3 Self-supervised learning with Kernel Dependence Maximization

Our method builds on the self-supervised learning framework used by most of the recent self-supervised learning approaches [16–19, 22, 24, 25]. For a dataset with  $N$  points  $x_i$ , each point goes through a random transformation  $t^p(x_i)$  (e.g. random crop), and then forms a feature representation  $z_i^p = f_\theta(t^p(x_i))$  with an encoder network  $f_\theta$ . We associate each image  $x_i$  with its identity  $y_i$ , which works as a one-hot encoded label:  $y_i \in \mathbb{R}^N$  and  $(y_i)_d = 1$  iff  $d = i$  (and zero otherwise). To match the transformations and image identities, we maximize the dependence between  $z_i$  and  $y_i$  such that  $z_i$  is predictive of its original image. To build representations suitable for downstream tasks, we also need to penalize high-variance representations. These ideas come together in our HSIC-based objective for self-supervised learning, which we term SSL-HSIC:

$$\mathcal{L}_{\text{SSL-HSIC}}(\theta) = -\text{HSIC}(Z, Y) + \gamma \sqrt{\text{HSIC}(Z, Z)}. \quad (4)$$

Unlike contrastive losses, which make the  $z_i^p$  from the same  $x_i$  closer and those from different  $x_j$  more distant, we propose an alternative way to match different transformations of the same image with its *abstract identity* (e.g. position in the dataset).

Our objective also resembles the HSIC bottleneck for supervised learning [27] (in particular, the version of [28]), but ours uses a square root for  $\text{HSIC}(Z, Z)$ . The square root makes the two terms on the same scale:  $\text{HSIC}(Z, Y)$  is effectively a dot product, and  $\sqrt{\text{HSIC}(Z, Z)}$  a norm, so that e.g. scaling the kernel by a constant does not change the relative amount of regularization;<sup>2</sup> this also gives better performance in practice.

Due to the one-hot encoded labels, we can re-write  $\text{HSIC}(Z, Y)$  as (see Appendix A)

$$\text{HSIC}(Z, Y) \propto \mathbb{E}_{z_1, z_2 \sim \text{pos}} [k(z_1, z_2)] - \mathbb{E}_{z_1} \mathbb{E}_{z_2} [k(z_1, z_2)], \quad (5)$$

<sup>1</sup>In a slight abuse of notation, we use  $\phi(x)\psi(y)^\top$  for the tensor product  $\phi(x) \otimes \psi(y) \in \mathcal{F} \otimes \mathcal{G}$ .

<sup>2</sup>Other prior work on maximizing HSIC [41, 45] used  $\text{HSIC}(Z, Y) / \sqrt{\text{HSIC}(Z, Z) \text{HSIC}(Y, Y)}$ , or equivalently [46] the distance correlation [47]; the kernel-target alignment [48, 49] is also closely related. Here, the overall scale of either kernel does not change the objective. Our  $\text{HSIC}(Y, Y)$  is constant (hence absorbed in  $\gamma$ ), and we found an additive penalty to be more stable in optimization than dividing the estimators.

where the first expectation is over the distribution of “positive” pairs (those from the same source image), and the second one is a sum over all image pairs, including their transformations. The first term in (5) pushes representations belonging to the same image identity together, while the second term keeps mean representations for each identity apart (as in Figure 2). The scaling of  $\text{HSIC}(Z, Y)$  depends on the choice of the kernel over  $Y$ , and is irrelevant to the optimization.

This form also reveals three key theoretical results. Section 3.1 shows that InfoNCE is better understood as an HSIC-based loss than a mutual information between views. Section 3.2 reveals that the dependence maximization in  $\text{HSIC}(Z, Y)$  can also be viewed as a form of distance metric learning, where the cluster structure is defined by the labels. Finally,  $\text{HSIC}(Z, Y)$  is proportional to the average kernel-based distance between the distribution of views for each source image (the maximum mean discrepancy, MMD; see Appendix B.2).

### 3.1 Connection to InfoNCE

In this section we show the connection between InfoNCE and our loss; see Appendix B for full details. We first write the latter in its infinite sample size limit (see [23] for a derivation) as

$$\mathcal{L}_{\text{InfoNCE}}(\theta) = -\mathbb{E}_{z_1, z_2 \sim \text{pos}} [k(z_1, z_2)] + \mathbb{E}_{z_1} \log \mathbb{E}_{z_2} [\exp(k(z_1, z_2))] , \quad (6)$$

where the last two expectations are taken over all points, and the first is over the distribution of positive pairs. The kernel  $k(z_1, z_2)$  was originally formulated as a scoring function in a form of a dot product [15], and then a scaled cosine similarity [19]. Both functions are valid kernels.

Now assume that  $k(z_1, z_2)$  doesn’t deviate much from  $\mathbb{E}_{z_2} [k(z_1, z_2)]$ , Taylor-expand the exponent in (6) around  $\mathbb{E}_{z_2} [k(z_1, z_2)]$ , then expand  $\log(1 + \mathbb{E}_{z_2}(\dots)) \approx \mathbb{E}_{z_2}(\dots)$ . We obtain an  $\text{HSIC}(Z, Y)$ -based objective:

$$\mathcal{L}_{\text{InfoNCE}}(\theta) \approx \underbrace{-\mathbb{E}_{z_1, z_2 \sim \text{pos}} [k(z_1, z_2)] + \mathbb{E}_{z_1} \mathbb{E}_{z_2} [k(z_1, z_2)]}_{\propto -\text{HSIC}(Z, Y)} + \frac{1}{2} \underbrace{\mathbb{E}_{z_1} [\text{Var}_{z_2} [k(z_1, z_2)]]}_{\text{variance penalty}} . \quad (7)$$

Since the scaling of  $\text{HSIC}(Z, Y)$  is irrelevant to the optimization, we assume scaling to replace  $\propto$  with  $=$ . In the small variance regime, we can show that for the right  $\gamma$ ,

$$-\text{HSIC}(Z, Y) + \gamma \text{HSIC}(Z, Z) \leq \mathcal{L}_{\text{InfoNCE}}(\theta) + o(\text{variance}) . \quad (8)$$

For  $\text{HSIC}(Z, Z) \leq 1$ , we also have that

$$-\text{HSIC}(Z, Y) + \gamma \text{HSIC}(Z, Z) \leq \mathcal{L}_{\text{SSL-HSIC}}(\theta) \quad (9)$$

due to the square root. InfoNCE and SSL-HSIC in general don’t quite bound each other due to discrepancy in the variance terms, but in practice the difference is small.

Why should we prefer the HSIC interpretation of InfoNCE? Initially, InfoNCE was suggested as a variational approximation to the mutual information between two views [15]. It has been observed, however, that using tighter estimators of mutual information leads to worse performance [30]. It is also simple to construct examples where InfoNCE finds different representations while the underlying MI remains constant [30]. Alternative theories suggest that InfoNCE balances alignment of “positive” examples and uniformity of the overall feature representation [23], or that (under strong assumptions) it can identify the latent structure in a hypothesized data-generating process, akin to nonlinear ICA [50]. Our view is consistent with these theories, but doesn’t put restrictive assumptions on the input data or learned representations. In Section 5 (summarized in Table 8a), we show that our interpretation gives rise to a better objective in practice.

### 3.2 Connection to metric learning

Our SSL-HSIC objective is closely related to kernel alignment [48], especially centered kernel alignment [49]. As a kernel method for distance metric learning, kernel alignment measures the agreement between a kernel function and a target function. Intuitively, the self-supervised labels  $Y$  imply a cluster structure, and  $\text{HSIC}(Z, Y)$  estimates the degree of agreement between the learned features and this cluster structure in the kernel space. This relationship with clustering is also



established in [40, 41, 45], where labels are learned rather than features. The clustering perspective is more evident when we assume linear kernels over both  $Z$  and  $Y$ , and  $Z$  is unit length and centered.<sup>3</sup>

$$\begin{aligned} -\text{HSIC}(Z, Y) &\propto -\frac{1}{M} \text{Tr}(Y^\top Z^\top Z Y) + \text{Tr}(Z^\top Z) - NM \\ &= -\frac{1}{M} \sum_{i=1}^N \left\| \sum_{p=1}^M z_i^p \right\|_2^2 + \sum_{i=1}^N \sum_{p=1}^M \|z_i^p\|_2^2 - NM = \sum_{i=1}^N \sum_{p=1}^M \|z_i^p - \bar{z}_i\|_2^2 - NM, \end{aligned} \quad (10)$$

with  $M$  the number of augmentations per image and  $\bar{z}_i = \sum_p z_i^p / M$  the average feature vector of the augmented views of  $x_i$ . We emphasize, though, that (10) assumes centered, normalized data with linear kernels; the right-hand side of (10) could be optimized by setting all  $z_i^p$  to the same vector for each  $i$ , but this does not actually optimize  $\text{HSIC}(Z, Y)$ .

Equation (10) shows that we recover the spectral formulation [51] and sum-of-squares loss used in the k-means clustering algorithm from the kernel objective. Moreover, the self-supervised label imposes that the features from transformations of the same image are gathered in the same cluster. Equation (10) also allows us to connect SSL-HSIC to non-contrastive objectives such as BYOL, although the connection is subtle because of its use of predictor and target networks. If each image is augmented with two views, we can compute (10) using  $\bar{z}_i \approx (z_i^1 + z_i^2) / 2$ , so the clustering loss becomes  $\propto \sum_i \|z_i^1 - z_i^2\|_2^2$ . This is exactly the BYOL objective, only that  $z_i^2$  in BYOL comes from a target network. The assumption of centered and normalized features for (10) is important in the case of BYOL: without it, BYOL can find trivial solutions where all the features are collapsed to the same feature vector far away from the origin. The target network is used to prevent the collapse. SSL-HSIC, on the other hand, rules out such a solution by building the centering into the loss function, and therefore can be trained successfully without a target network or stop gradient operation.

### 3.3 Estimator of SSL-HSIC

To use SSL-HSIC, we need to correctly and efficiently estimate (4). Both points are non-trivial: the self-supervised framework implies non-i.i.d. batches (due to positive examples), while the estimator in (3) assumes i.i.d. data; moreover, the time to compute (3) is quadratic in the batch size.

First, for  $\text{HSIC}(Z, Z)$  we use the biased estimator in (3). Although the i.i.d. estimator (3) results in an  $O(1/B)$  bias for  $B$  original images in the batch size (see Appendix A), the batch size  $B$  is large in our case and therefore the bias is negligible. For  $\text{HSIC}(Z, Y)$  the situation is more delicate: the i.i.d. estimator needs re-scaling, and its bias depends on the number of positive examples  $M$ , which is typically very small (usually 2). We propose the following estimator:

$$\widehat{\text{HSIC}}(Z, Y) = \frac{\Delta l}{N} \left( \frac{1}{BM(M-1)} \sum_{ipl} k(z_i^p, z_i^l) - \frac{1}{B^2 M^2} \sum_{ijpl} k(z_i^p, z_j^l) - \frac{1}{M-1} \right), \quad (11)$$

where  $i$  and  $j$  index original images, and  $p$  and  $l$  their random transformations;  $k$  is the kernel used for latent  $Z$ ,  $l$  is the kernel used for the labels, and  $\Delta l = l(i, i) - l(i, j)$  ( $l$  for same labels minus  $l$  for different labels). Note that due to the one-hot structure of self-supervised labels  $Y$ , the standard (i.i.d.-based) estimator would miss the  $1/N$  scaling and the  $M-1$  correction (the latter is important in practice, as we usually have  $M=2$ ). See Appendix A for the derivations.

For convenience, we assume  $\Delta l = N$  (any scaling of  $l$  can be subsumed by  $\gamma$ ), and optimize

$$\hat{\mathcal{L}}_{\text{SSL-HSIC}}(\theta) = -\widehat{\text{HSIC}}(Z, Y) + \gamma \sqrt{\widehat{\text{HSIC}}(Z, Z)}. \quad (12)$$

The computational complexity of the proposed estimators is  $O(B^2 M^2)$  for each mini-batch of size  $B$  with  $M$  augmentations. We can reduce the complexity to  $O(BM)$  by using random Fourier features (RFF) [33], which approximate the kernel  $k(z_1, z_2)$  with a carefully chosen random  $D$ -dimensional approximation  $R(z_1)^\top R(z_2)$  for  $R(z) : \mathbb{R}^{D_z} \rightarrow \mathbb{R}^D$ , such that  $k(z_1, z_2) = \mathbb{E} [R(z_1)^\top R(z_2)]$ . Fourier frequencies are sampled independently for the two kernels on  $Z$  in  $\text{HSIC}(Z, Z)$  at each training step. We leave the details on how to construct  $R(z)$  for the kernels we use to Appendix C.

<sup>3</sup>Centered  $Z$  is a valid assumption for BYOL, as the target network keeps representations of views with different image identities away from each other. For high-dimensional unit vectors, this can easily lead to orthogonal representations. We also observe centered representations empirically: see Appendix B.3.

## 4 Experiments

In this section, we present our experimental setup, where we assess the performance of the representation learned with SSL-HSIC both with and without a target network. First, we train a model with a standard ResNet-50 backbone using SSL-HSIC as objective on the training set of ImageNet ILSVRC-2012 [1]. For evaluation, we retain the backbone as a feature extractor for downstream tasks. We evaluate the representation on various downstream tasks including classification, object segmentation, object detection and depth estimation.

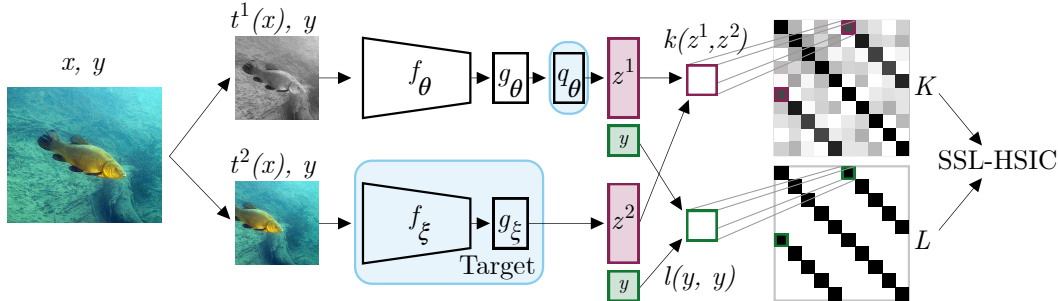


Figure 4: Architecture and SSL-HSIC objective. A self-supervised label  $y$  – an indicator of the image identity – is associated with an image  $x$ . Image transformation functions  $t$  are sampled and applied to the original image, resulting in views  $t^1(x)$  and  $t^2(x)$ . Features  $z^1$  and  $z^2$  are obtained after passing the augmented views through encoder ( $f$ ), projector ( $g$ ), and possibly predictor ( $q$ ) networks, while label  $y$  is retained. Kernel matrices,  $K$  for the latents and  $L$  for the labels, are computed on the mini-batch of data; SSL-HSIC is estimated with  $K$  and  $L$  as in (12). The blue boxes reflect two potential options: when using a target network,  $\xi$  is a moving average of  $\theta$ , and a predictor network  $q$  is added; without the target network,  $q$  is removed and  $\xi$  is simply equal to  $\theta$ .

### 4.1 Implementation

**Architecture** Figure 4 illustrates the architecture we used for SSL-HSIC in this section. To facilitate comparison between different methods, our encoder  $f_\theta$  uses the standard ResNet-50 backbone without the final classification layer. The output of the encoder is a 2048-dimension embedding vector, which is the representation used for downstream tasks. As in BYOL [25], our projector  $g$  and predictor  $q$  networks are 2-layer MLPs with 4096 hidden dimensions and 256 output dimensions. The outputs of the networks are batch-normalized and rescaled to unit norm before computing the loss. We use an inverse multiquadric kernel (IMQ) for the latent representation (approximated with 512 random Fourier features that are resampled at each step; see Appendix C for details) and a linear kernel for labels.  $\gamma$  in (4) is set to 3. When training without a target network, unlike SimSiam [24], we do not stop gradients for either branch. If the target network is used, its weights are an exponential moving average of the online network weights. We employ the same schedule as BYOL [25],  $\tau = 1 - 0.01 \cdot (\cos(\pi t/T) + 1)/2$  with  $t$  the current step and  $T$  the total training steps.

**Image augmentation** Our method uses the same data augmentation scheme as BYOL (see Appendix D.1). Briefly, we first draw a random patch from the original image and resize it to  $224 \times 224$ . Then, we apply a random horizontal flip, followed by color jittering, consisting of a random sequence of brightness, contrast, saturation, hue adjustments, and an optional grayscale conversion. Finally Gaussian blur and solarization are applied, and the view is normalized with ImageNet statistics.

**Optimization** We train the model with a batch size of 4096 on 128 Cloud TPU v4 cores. Again, following [19, 25], we use the LARS optimizer [52] with a cosine decay learning rate schedule over 1000 epochs. The base learning rate to all of our experiments is 0.4 and it is scaled linearly [53] with the batch size  $lr = 0.4 \times \text{batch\_size}/256$ . All experiments use weight decay of  $10^{-6}$ .

**Learning kernel parameters** We use a linear kernel for labels, since the type of kernel only scales (12). Our inverse multiquadric kernel for the latent  $Z$  has an additional kernel scale parameter. We optimize this along with all other parameters, but regularize it to maximize the entropy of the distribution  $k_\sigma(s)$ , where  $s_{ij} = \|z_i - z_j\|^2$ ; this amounts to maximizing  $\log \|k'_\sigma(s)\|^2$  (Appendix D.1.2).

## 4.2 Evaluation Results

**Linear evaluation on ImageNet** Learned features are evaluated with the standard linear evaluation protocol commonly used in evaluating self-supervised learning methods [15–22, 25]. Table 1 reports the top-1 and top-5 accuracies obtained with SSL-HSIC on ImageNet validation set, and compares to previous self-supervised learning methods. Without a target network, our method reaches 72.2% top-1 and 90.7% top-5 accuracies. Unlike BYOL, the SSL-HSIC objective prevents the network from finding trivial solutions as explained in Section 3.2. Adding the target network, our method outperforms most previous methods, achieving top-1 accuracy of 74.8% and top-5 accuracy of 92.2%. The fact that we see performance gains from adopting a target network suggests that its effect is not yet well understood, although note discussion in [25] which points to its stabilizing effect.

Table 1: Linear evaluation on the ImageNet validation set.

	Top-1(%)	Top-5(%)
Supervised [54]	75.9	92.8
SimCLR [19]	69.3	89.0
MoCo v2 [20]	71.1	90.1
BYOL [25]	74.3	91.6
SwAV [18]	<b>75.3</b>	-
Barlow Twins [22]	73.2	91.0
SSL-HSIC (w/o target)	72.2	90.7
SSL-HSIC (w/ target)	74.8	<b>92.2</b>

Table 2: Fine-tuning on 1%, 10% and 100% of the ImageNet training set and evaluating on the validation set.

	Top-1(%)			Top-5(%)		
	1%	10%	100%	1%	10%	100%
Supervised [54]	25.4	56.4	75.9	48.4	80.4	92.8
SimCLR [19]	48.3	65.6	76.0	75.5	87.8	93.1
BYOL [25]	53.2	68.8	<b>77.7</b>	78.4	89.0	<b>93.9</b>
SwAV [18]	53.9	<b>70.2</b>	-	78.5	<b>89.9</b>	-
Barlow Twins [22]	<b>55.0</b>	69.7	-	<b>79.2</b>	89.3	-
SSL-HSIC (w/o target)	45.3	65.5	76.4	72.7	87.5	93.2
SSL-HSIC (w/ target)	52.1	67.9	77.2	77.7	88.6	93.6

**Semi-supervised learning on ImageNet** We fine-tune the network pretrained with SSL-HSIC on 1%, 10% and 100% of ImageNet, using the same ImageNet splits as SimCLR [19]. Table 2 summarizes the semi-supervised learning performance. Our method, with or without a target network, has competitive performance in both data regimes. The target network has the most impact on the small-data regime, with 1% labels.

Table 3: Comparison of transfer learning performance on 12 image datasets. Supervised-IN is trained on ImageNet with supervised pretraining. Random init trains on individual dataset with randomly initialized weights. MPCA refers to mean per-class accuracy; AP50 is average precision at IoU=0.5.

Dataset	Birdsnap	Caltech101	Cifar10	Cifar100	DTD	Aircraft	Food	Flowers	Pets	Cars	SUN397	VOC2007
Metric	Top-1	MPCA	Top-1	Top-1	Top-1	MPCA	Top-1	MPCA	MPCA	Top-1	Top-1	AP50
<i>Linear:</i>												
Supervised-IN [19]	53.7	<b>94.5</b>	<b>93.6</b>	78.3	74.9	<b>61.0</b>	72.3	94.7	<b>91.5</b>	<b>67.8</b>	<b>61.9</b>	82.8
SimCLR [19]	37.4	90.3	90.6	71.6	74.5	50.3	68.4	90.3	83.6	50.3	58.8	80.5
BYOL [25]	57.2	94.2	91.3	<b>78.4</b>	75.5	60.6	75.3	<b>96.1</b>	90.4	66.7	62.2	82.5
SSL-HSIC (w/o target)	50.6	92.3	91.5	75.9	75.3	57.9	73.6	95.0	88.2	59.3	61.0	81.4
SSL-HSIC (w/ target)	<b>57.8</b>	93.5	92.3	77.0	<b>76.2</b>	58.5	<b>75.6</b>	95.4	91.2	62.6	61.8	<b>83.3</b>
<i>Fine-tuned:</i>												
Supervised-IN [19]	75.8	93.3	97.5	<b>86.4</b>	74.6	86.0	88.3	<b>97.6</b>	<b>92.1</b>	<b>92.1</b>	<b>94.3</b>	85.0
Random init [19]	<b>76.1</b>	72.6	95.9	80.2	64.8	85.9	86.9	92.0	81.5	91.4	53.6	67.3
SimCLR [19]	75.9	92.1	97.7	85.9	73.2	88.1	88.2	97.0	89.2	91.3	63.5	84.1
BYOL [25]	76.3	<b>93.8</b>	<b>97.8</b>	86.1	<b>76.2</b>	88.1	<b>88.5</b>	97.0	91.7	91.6	63.7	<b>85.4</b>
SSL-HSIC (w/o target)	73.1	91.5	97.4	85.3	75.3	87.1	87.5	96.4	90.6	91.6	62.2	84.1
SSL-HSIC (w/ target)	74.9	<b>93.8</b>	<b>97.8</b>	84.7	75.4	<b>88.9</b>	87.7	97.3	91.7	91.8	61.7	84.1

**Transfer to other classification tasks** To investigate the generality of the representation learned with SSL-HSIC, we evaluate the transfer performance for classification on 12 natural image datasets [55–64] using the same procedure as [19, 25, 65]. Table 3 shows the top-1 accuracy of the linear evaluation and fine-tuning performance on the test set. SSL-HSIC gets state-of-the-art performance on 3 of the classification tasks and reaches strong performance on others for this benchmark, indicating the learned representations are robust for transfer learning.

**Transfer to other vision tasks** To test the ability of transferring to tasks other than classification, we fine-tune the network on semantic segmentation, depth estimation and object detection tasks. We use Pascal VOC2012 dataset [58] for semantic segmentation, NYU v2 dataset [66] for depth estimation and COCO [67] for object detection. Object detection outputs either bounding box or object segmentation (instance segmentation). Details of the evaluations setup is in Appendix D.2. Table 4 and Table 5 shows that SSL-HSIC achieves competitive performance on all three vision tasks.



Table 4: Fine-tuning performance on semantic segmentation and depth estimation. Mean Intersection over Union (mIoU) is reported for semantic segmentation. Relative error (rel), root mean squared error (rms), and the percent of pixels (pct) where the error is below  $1.25^n$  thresholds are reported for depth estimation.

Method	VOC2012		NYU v2			rms	rel
	mIoU	pct.< 1.25	pct.< 1.25 <sup>2</sup>	pct.< 1.25 <sup>3</sup>			
Supervised-IN	74.4	81.1	95.3	98.8	0.573	<b>0.127</b>	
SimCLR	75.2	83.3	96.5	99.1	0.557	0.134	
BYOL	<b>76.3</b>	<b>84.6</b>	96.7	99.1	0.541	0.129	
SSL-HSIC(w/o target)	74.9	84.1	96.7	<b>99.2</b>	<b>0.539</b>	0.130	
SSL-HSIC(w/ target)	76.0	83.8	<b>96.8</b>	99.1	0.548	0.130	

Table 5: Fine-tuning performance on COCO object detection tasks. Precision, averaged over 10 IoU (Intersection over Union) thresholds, is reported for both bounding box and object segmentation.

Method	AP <sup>bb</sup>	AP <sup>mk</sup>
Supervised	39.6	35.6
SimCLR	39.7	35.8
MoCo v2	40.1	36.3
BYOL	<b>41.6</b>	37.2
SwAV	<b>41.6</b>	<b>37.8</b>
SSL-HSIC(w/o target)	40.5	36.3
SSL-HSIC(w/ target)	41.3	36.8

## 5 Ablation Studies

We present ablation studies to gain more intuition on SSL-HSIC. Here, we use a ResNet-50 backbone trained for 100 epochs on ImageNet, and evaluate with the linear protocol unless specified.

**ResNet architectures** In this ablation, we investigate the performance of SSL-HSIC with wider and deeper ResNet architecture. Figure 1 and Table 6 show our main results. The performance of SSL-HSIC gets better with larger networks. We used the supervised baseline from [25] which our training framework is based on ([19] reports lower performance). The performance gap between SSL-HSIC and the supervised baseline diminishes with larger architectures. In addition, Table 7 presents the semi-supervised learning results with subsets 1%, 10% and 100% of the ImageNet data.

Table 6: Top-1 and top-5 accuracies for different ResNet architectures using linear evaluation protocol.

ResNet	SSL-HSIC		BYOL[25]		Sup.[25]	
	Top1	Top5	Top1	Top5	Top1	Top5
50 (1x)	74.8	92.2	74.3	91.6	76.4	92.9
50 (2x)	77.9	94.0	77.4	93.6	79.9	95.0
50 (4x)	79.1	94.5	78.6	94.2	80.7	95.3
200 (2x)	79.6	94.8	79.6	94.9	80.1	95.2

Table 7: Top-1 and top-5 accuracies for different ResNet architectures using semi-supervised fine-tuning.

ResNet	Top1			Top5		
	1%	10%	100%	1%	10%	100%
50 (1x)	52.1	67.9	77.2	77.7	88.6	93.6
50 (2x)	61.2	72.6	79.3	83.8	91.2	94.7
50 (4x)	67.0	75.4	79.7	87.4	92.5	94.8
200(2x)	69.0	76.3	80.5	88.3	92.9	95.2

**Regularization term** We compare performance of InfoNCE with SSL-HSIC in Table 8a since they can be seen as approximating the same  $\text{HSIC}(Z, Y)$  objective but with different forms of regularization. We reproduce the InfoNCE result in our codebase, using the same architecture and data augmentation as for SSL-HSIC. Trained for 100 epochs (without a target network), InfoNCE achieves 66.0% top-1 and 86.9% top-5 accuracies, which is better than the result reported in [19]. For comparison, SSL-HSIC reaches 66.7% top-1 and 87.6% top-5 accuracies. This suggests that the regularization employed by SSL-HSIC is more effective.

**Kernel type** We investigate the effect of using different a kernel on latents  $Z$ . Training without a target network or random Fourier feature approximation, the top-1 accuracies for linear, Gaussian, and inverse multiquadric (IMQ) kernels are 65.27%, 66.67% and 66.72% respectively. Non-linear kernels indeed improve the performance; Gaussian and IMQ kernels reach very similar performance for 100 epochs. We choose IMQ kernel for longer runs, because its heavy-tail property can capture more signal when points are far apart.

**Number of RFF Features** Table 8b shows the performance of SSL-HSIC with different numbers of Fourier features. The RFF approximation has a minor impact on the overall performance, as long as we resample them; fixed sets of features performed poorly. Our main result picked 512 features, for substantial computational savings with minor loss in accuracy.

**Batch size** Similar to most of the self-supervised learning methods [19, 25], SSL-HSIC benefits from using a larger batch size during training. However, the drop of performance from using smaller batch size is not as pronounced as it is in SimCLR[19] as shown in Table 8c.

Table 8: Linear evaluation results when varying different hyperparameters.

(a) Regularization			(b) # Fourier features		(c) Batch size			(d) Projector/predictor size	
	Top-1	Top-5	# RFFs	Top-1(%)		Top-1(%)		Output Dim	Top-1(%)
SSL-HSIC	66.7	87.6	64	66.0	Batch Size	SSL-HSIC	SimCLR	64	65.4
InfoNCE	66.0	86.9	128	66.2				128	66.0
			256	66.2	256	63.7	57.5	256	66.4
			512	66.4	512	65.6	60.7	512	66.6
			1024	66.5	1024	66.7	62.8	1024	66.6
			2048	66.5	2048	67.1	64.0		
			No Approx.	66.7	4096	66.7	64.6		

**Projector and predictor output size** Table 8d shows the performance when using different output dimension for the projector/predictor networks. The performance saturates at 512 dimensions.

## 6 Conclusions

We introduced SSL-HSIC, a loss function for self-supervised representation learning based on kernel dependence maximization. We provided a unified view on various self-supervised learning losses: we proved that InfoNCE, a lower bound of mutual information, actually approximates SSL-HSIC with a variance-based regularization, and we can also interpret SSL-HSIC as metric learning where the cluster structure is imposed by the self-supervised label, of which the BYOL objective is a special case. We showed that training with SSL-HSIC achieves performance on par with the state-of-the-art on the standard self-supervised benchmarks.

Although using the image identity as self-supervised label provides a good inductive bias, it might not be wholly satisfactory; we expect that some images pairs are in fact more similar than others, based e.g. on their ImageNet class label. It will be interesting to explore methods that combine label structure discovery with representation learning (as in SwAV [18]). In this paper, we only explored learning image representations, but in future work SSL-HSIC can be extended to learning structure for  $Y$  as well, building on existing work [41, 45].

### Broader impact

Our work concentrates on providing a more theoretically grounded and interpretable loss function for self-supervised learning. A better understanding of self-supervised learning, especially through more interpretable learning dynamics, is likely to lead to better and more explicit control over societal biases of these algorithms. SSL-HSIC yields an alternative, clearer understanding of existing self-supervised methods. As such, it is unlikely that our method introduces further biases than those already present for self-supervised learning.

The broader impacts of the self-supervised learning framework is an area that has not been studied by the AI ethics community, but we think it calls for closer inspection. An important concern for fairness of ML algorithms is dataset bias. ImageNet is known for a number of problems such as offensive annotations, non-visual concepts and lack of diversity, in particular for underrepresented groups. Existing works and remedies typically focus on label bias. Since SSL doesn't use labels, however, the type and degree of bias could be very different from that of supervised learning. To mitigate the risk of dataset bias, one could employ dataset re-balancing to correct sampling bias [68] or completely exclude human images from the dataset while achieving the same performance [69].

A new topic to investigate for self-supervised learning is how the bias/unbiased representation could be transferred to downstream tasks. We are not aware of any work in this direction. Another area of concern is security and robustness. Compared to supervised learning, self-supervised learning typically involves more intensive data augmentation such as color jittering, brightness adjustment, etc. There is some initial evidence suggesting self-supervised learning improves model robustness [70]. However, since data augmentation can either be beneficial [71] or detrimental [72] depending on the type of adversarial attacks, more studies are needed to assess its role for self-supervised learning.

## Acknowledgments and Disclosure of Funding

The authors would like to thank Olivier J. Hénaff for valuable feedback on the manuscript and the help for evaluating object detection task. We thank Aaron Van den Oord and Oriol Vinyals for providing valuable feedback on the manuscript. We are grateful to Yonglong Tian, Ting Chen and the BYOL authors for the help with reproducing baselines and evaluating downstream tasks.

This work was supported by DeepMind, the Gatsby Charitable Foundation, the Wellcome Trust, NSERC, and the Canada CIFAR AI Chairs program.

## References

- [1] O. Russakovsky, J. Deng, H. Su, J. Krause, S. Satheesh, S. Ma, Z. Huang, A. Karpathy, A. Khosla, M. Bernstein, A. C. Berg, and L. Fei-Fei. “ImageNet large scale visual recognition challenge.” *International Journal of Computer Vision* 115.3 (2015), pp. 211–252.
- [2] G. E. Hinton and R. R. Salakhutdinov. “Reducing the dimensionality of data with neural networks.” *Science* 313.5786 (2006), pp. 504–507.
- [3] P. Vincent, H. Larochelle, I. Lajoie, Y. Bengio, P.-A. Manzagol, and L. Bottou. “Stacked denoising autoencoders: Learning useful representations in a deep network with a local denoising criterion.” *Journal of Machine Learning Research* 11.12 (2010).
- [4] A. Coates and A. Y. Ng. “Learning feature representations with k-means.” *Neural networks: Tricks of the trade*. Springer, 2012, pp. 561–580.
- [5] I. Higgins, L. Matthey, A. Pal, C. Burgess, X. Glorot, M. Botvinick, S. Mohamed, and A. Lerchner. “beta-VAE: Learning basic visual concepts with a constrained variational framework.” *ICLR*. 2016.
- [6] A. van den Oord, O. Vinyals, and K. Kavukcuoglu. “Neural Discrete Representation Learning.” *NeurIPS*. 2017. arXiv: [1711.00937](https://arxiv.org/abs/1711.00937).
- [7] W. Grathwohl, R. T. Q. Chen, J. Bettencourt, and D. Duvenaud. “Scalable Reversible Generative Models with Free-form Continuous Dynamics.” *ICLR*. 2019. arXiv: [1810.01367](https://arxiv.org/abs/1810.01367).
- [8] T. B. Brown, B. Mann, N. Ryder, M. Subbiah, J. Kaplan, P. Dhariwal, A. Neelakantan, P. Shyam, G. Sastry, A. Askell, S. Agarwal, A. Herbert-Voss, G. Krueger, T. Henighan, R. Child, A. Ramesh, D. M. Ziegler, J. Wu, C. Winter, C. Hesse, M. Chen, E. Sigler, M. Litwin, S. Gray, B. Chess, J. Clark, C. Berner, S. McCandlish, A. Radford, I. Sutskever, and D. Amodei. “Language Models are Few-Shot Learners.” *NeurIPS*. 2020. arXiv: [2005.14165](https://arxiv.org/abs/2005.14165).
- [9] C. Doersch, A. Gupta, and A. A. Efros. “Unsupervised Visual Representation Learning by Context Prediction.” *ICCV*. 2015. arXiv: [1505.05192](https://arxiv.org/abs/1505.05192).
- [10] G. Larsson, M. Maire, and G. Shakhnarovich. “Learning representations for automatic colorization.” *ECCV*. Springer. 2016, pp. 577–593.
- [11] M. Norouzi and P. Favaro. “Unsupervised learning of visual representations by solving jigsaw puzzles.” *ECCV*. Springer. 2016, pp. 69–84.
- [12] D. Pathak, P. Krahenbuhl, J. Donahue, T. Darrell, and A. A. Efros. “Context encoders: Feature learning by inpainting.” *CVPR*. 2016, pp. 2536–2544.
- [13] R. Zhang, P. Isola, and A. A. Efros. “Colorful image colorization.” *ECCV*. Springer. 2016, pp. 649–666.
- [14] S. Gidaris, P. Singh, and N. Komodakis. “Unsupervised representation learning by predicting image rotations.” *ICLR*. 2018. arXiv: [1803.07728](https://arxiv.org/abs/1803.07728).
- [15] A. van den Oord, Y. Li, and O. Vinyals. “Representation learning with contrastive predictive coding.” 2018. arXiv: [1807.03748](https://arxiv.org/abs/1807.03748).
- [16] P. Bachman, R. D. Hjelm, and W. Buchwalter. “Learning representations by maximizing mutual information across views.” *NeurIPS*. 2019. arXiv: [1906.00910](https://arxiv.org/abs/1906.00910).
- [17] K. He, H. Fan, Y. Wu, S. Xie, and R. B. Girshick. “Momentum Contrast for Unsupervised Visual Representation Learning.” *CVPR*. 2019. arXiv: [1911.05722](https://arxiv.org/abs/1911.05722).
- [18] M. Caron, I. Misra, J. Mairal, P. Goyal, P. Bojanowski, and A. Joulin. “Unsupervised learning of visual features by contrasting cluster assignments.” *NeurIPS*. 2020. arXiv: [2006.09882](https://arxiv.org/abs/2006.09882).
- [19] T. Chen, S. Kornblith, M. Norouzi, and G. Hinton. “A Simple Framework for Contrastive Learning of Visual Representations.” *ICML*. 2020. arXiv: [2002.05709](https://arxiv.org/abs/2002.05709).

- [20] X. Chen, H. Fan, R. B. Girshick, and K. He. “Improved Baselines with Momentum Contrastive Learning.” 2020. arXiv: [2003.04297](#).
- [21] O. Henaff. “Data-efficient image recognition with contrastive predictive coding.” *ICML*. 2020. arXiv: [1905.09272](#).
- [22] J. Zbontar, L. Jing, I. Misra, Y. LeCun, and S. Deny. “Barlow Twins: Self-Supervised Learning via Redundancy Reduction.” 2021. arXiv: [2103.03230](#).
- [23] T. Wang and P. Isola. “Understanding Contrastive Representation Learning through Alignment and Uniformity on the Hypersphere.” 2020. arXiv: [2005.10242](#).
- [24] X. Chen and K. He. “Exploring Simple Siamese Representation Learning.” 2020. arXiv: [2011.10566](#).
- [25] J.-B. Grill, F. Strub, F. Altché, C. Tallec, P. H. Richemond, E. Buchatskaya, C. Doersch, B. A. Pires, Z. D. Guo, M. G. Azar, B. Piot, K. Kavukcuoglu, R. Munos, and M. Valko. “Bootstrap Your Own Latent: A New Approach to Self-Supervised Learning.” *NeurIPS*. 2020. arXiv: [2006.07733](#).
- [26] A. Gretton, O. Bousquet, A. Smola, and B. Schölkopf. “Measuring statistical dependence with Hilbert-Schmidt norms.” *ALT*. Springer. 2005, pp. 63–77.
- [27] K. W.-D. Ma, J. P. Lewis, and W. B. Kleijn. “The HSIC Bottleneck: Deep Learning without Back-Propagation.” *AAAI*. 2020.
- [28] R. Pogodin and P. Latham. “Kernelized information bottleneck leads to biologically plausible 3-factor Hebbian learning in deep networks.” *NeurIPS* (2020).
- [29] N. Tishby and N. Zaslavsky. “Deep Learning and the Information Bottleneck Principle.” *IEEE Information Theory Workshop*. 2015. arXiv: [1503.02406](#).
- [30] M. Tschannen, J. Djolonga, P. K. Rubenstein, S. Gelly, and M. Lucic. “On mutual information maximization for representation learning.” *ICLR*. 2020. arXiv: [1907.13625](#).
- [31] I. Belghazi, S. Rajeswar, A. Baratin, R. D. Hjelm, and A. C. Courville. “MINE: Mutual Information Neural Estimation.” *ICML*. 2018. arXiv: [1801.04062](#).
- [32] B. Poole, S. Ozair, A. van den Oord, A. A. Alemi, and G. Tucker. “On Variational Bounds of Mutual Information.” *ICML*. 2019. arXiv: [1905.06922](#).
- [33] A. Rahimi and B. Recht. “Random Features for Large-Scale Kernel Machines.” *NeurIPS*. 2007.
- [34] T. Chen, S. Kornblith, K. Swersky, M. Norouzi, and G. Hinton. “Big Self-Supervised Models are Strong Semi-Supervised Learners.” *NeurIPS*. 2020. arXiv: [2006.10029](#).
- [35] Y.-H. H. Tsai, S. Bai, L.-P. Morency, and R. Salakhutdinov. “A note on connecting barlow twins with negative-sample-free contrastive learning.” *arXiv preprint arXiv:2104.13712* (2021).
- [36] T. Chen and L. Li. “Intriguing Properties of Contrastive Losses.” 2020. arXiv: [2011.02803](#).
- [37] Z. Szabó and B. K. Sriperumbudur. “Characteristic and Universal Tensor Product Kernels.” *Journal of Machine Learning Research* 18.233 (2018), pp. 1–29.
- [38] A. Gretton, K. Fukumizu, C. H. Teo, L. Song, B. Schölkopf, and A. J. Smola. “A kernel statistical test of independence.” *NeurIPS*. 2007.
- [39] L. Song, A. Smola, A. Gretton, J. Bedo, and K. Borgwardt. “Feature selection via dependence maximization.” *Journal of Machine Learning Research* 13.5 (2012).
- [40] L. Song, A. Smola, A. Gretton, and K. M. Borgwardt. “A Dependence Maximization View of Clustering.” *ICML*. 2007.
- [41] M. B. Blaschko and A. Gretton. “Learning Taxonomies by Dependence Maximization.” *NeurIPS*. 2009.
- [42] S. Jain, G. Liu, and D. Gifford. “Information Condensing Active Learning.” 2020. arXiv: [2002.07916](#).
- [43] D. Wu, Y. Zhao, Y.-H. H. Tsai, M. Yamada, and R. Salakhutdinov. “‘Dependency Bottleneck’ in Auto-encoding Architectures: an Empirical Study.” 2018. arXiv: [1802.05408](#).
- [44] A. Nøkland and L. H. Eidnes. “Training neural networks with local error signals.” *ICML*. 2019. arXiv: [1901.06656](#).
- [45] M. B. Blaschko, W. Zaremba, and A. Gretton. “Taxonomic Prediction with Tree-Structured Covariances.” *Machine Learning and Knowledge Discovery in Databases*. Springer Berlin Heidelberg, 2013, pp. 304–319.

- [46] D. Sejdinovic, B. Sriperumbudur, A. Gretton, and K. Fukumizu. “Equivalence of distance-based and RKHS-based statistics in hypothesis testing.” *The Annals of Statistics* 41.5 (2013), pp. 2263–2291.
- [47] G. J. Székely, M. L. Rizzo, and N. K. Bakirov. “Measuring and testing dependence by correlation of distances.” *The Annals of Statistics* 35.6 (2007), pp. 2769–2794.
- [48] N. Cristianini, J. Shawe-Taylor, A. Elisseeff, and J. Kandola. “On Kernel-Target Alignment.” *NeurIPS*. Vol. 14. 2002.
- [49] C. Cortes, M. Mohri, and A. Rostamizadeh. “Algorithms for learning kernels based on centered alignment.” *The Journal of Machine Learning Research* 13.1 (2012), pp. 795–828.
- [50] R. S. Zimmermann, Y. Sharma, S. Schneider, M. Bethge, and W. Brendel. “Contrastive Learning Inverts the Data Generating Process.” 2021. arXiv: [2102.08850](https://arxiv.org/abs/2102.08850).
- [51] H. Zha, X. He, C. Ding, M. Gu, and H. D. Simon. “Spectral relaxation for k-means clustering.” *NeurIPS*. 2001, pp. 1057–1064.
- [52] Y. You, I. Gitman, and B. Ginsburg. “Scaling SGD Batch Size to 32K for ImageNet Training.” 2017. arXiv: [1708.03888](https://arxiv.org/abs/1708.03888).
- [53] P. Goyal, P. Dollár, R. B. Girshick, P. Noordhuis, L. Wesolowski, A. Kyrola, A. Tulloch, Y. Jia, and K. He. “Accurate, Large Minibatch SGD: Training ImageNet in 1 Hour.” 2017. arXiv: [1706.02677](https://arxiv.org/abs/1706.02677).
- [54] X. Zhai, A. Oliver, A. Kolesnikov, and L. Beyer. “S<sup>4</sup>L: Self-Supervised Semi-Supervised Learning.” *ICCV*. 2019. arXiv: [1905.03670](https://arxiv.org/abs/1905.03670).
- [55] L. Fei-Fei, R. Fergus, and P. Perona. “Learning Generative Visual Models from Few Training Examples: An Incremental Bayesian Approach Tested on 101 Object Categories.” *CVPR Workshop*. 2004.
- [56] M.-E. Nilsback and A. Zisserman. “Automated flower classification over a large number of classes.” *2008 Sixth Indian Conference on Computer Vision, Graphics & Image Processing*. IEEE. 2008, pp. 722–729.
- [57] A. Krizhevsky. “Learning multiple layers of features from tiny images.” 2009. URL: <https://www.cs.toronto.edu/~kriz/learning-features-2009-TR.pdf>.
- [58] M. Everingham, L. Van Gool, C. K. Williams, J. Winn, and A. Zisserman. “The Pascal visual object classes (VOC) challenge.” *IJCV* 88.2 (2010), pp. 303–338.
- [59] J. Xiao, J. Hays, K. A. Ehinger, A. Oliva, and A. Torralba. “SUN database: Large-scale scene recognition from abbey to zoo.” *CVPR*. 2010.
- [60] O. M. Parkhi, A. Vedaldi, A. Zisserman, and C. V. Jawahar. “Cats and Dogs.” *CVPR*. 2012.
- [61] M. Cimpoi, S. Maji, I. Kokkinos, S. Mohamed, and A. Vedaldi. “Describing Textures in the Wild.” *CVPR*. 2013. arXiv: [1311.3618](https://arxiv.org/abs/1311.3618).
- [62] J. Krause, J. Deng, M. Stark, and L. Fei-fei. “Collecting a large-scale dataset of fine-grained cars. The Second Workshop on Fine-Grained Visual Categorization.” 2013.
- [63] L. Bossard, M. Guillaumin, and L. Van Gool. “Food-101—mining discriminative components with random forests.” *ECCV*. Springer. 2014, pp. 446–461.
- [64] S. Maji, E. Rahtu, J. Kannala, M. B. Blaschko, and A. Vedaldi. “Fine-Grained Visual Classification of Aircraft.” arXiv: [1306.5151](https://arxiv.org/abs/1306.5151).
- [65] S. Kornblith, J. Shlens, and Q. V. Le. “Do Better ImageNet Models Transfer Better?” *CVPR*. 2019. arXiv: [1805.08974](https://arxiv.org/abs/1805.08974).
- [66] N. Silberman, D. Hoiem, P. Kohli, and R. Fergus. “Indoor Segmentation and Support Inference from RGBD Images.” *ECCV*. 2012.
- [67] T.-Y. Lin, M. Maire, S. J. Belongie, L. D. Bourdev, R. B. Girshick, J. Hays, P. Perona, D. Ramanan, P. Dollár, and C. L. Zitnick. “Microsoft COCO: Common Objects in Context.” *ECCV*. 2014. arXiv: [1405.0312](https://arxiv.org/abs/1405.0312).
- [68] K. Yang, K. Qinami, L. Fei-Fei, J. Deng, and O. Russakovsky. “Towards fairer datasets: Filtering and balancing the distribution of the people subtree in the imagenet hierarchy.” *Proceedings of the 2020 Conference on Fairness, Accountability, and Transparency*. 2020, pp. 547–558.
- [69] Y. Asano, C. Rupprecht, A. Zisserman, and A. Vedaldi. “PASS: An ImageNet replacement for self-supervised pretraining without humans” (2021).



- [70] D. Hendrycks, M. Mazeika, S. Kadavath, and D. Song. “Using self-supervised learning can improve model robustness and uncertainty.” *arXiv preprint arXiv:1906.12340* (2019).
- [71] A. Sablayrolles, M. Douze, C. Schmid, Y. Ollivier, and H. Jégou. “White-box vs black-box: Bayes optimal strategies for membership inference.” *International Conference on Machine Learning*. PMLR, 2019, pp. 5558–5567.
- [72] D. Yu, H. Zhang, W. Chen, J. Yin, and T.-Y. Liu. “How Does Data Augmentation Affect Privacy in Machine Learning?” *Proceedings of the AAAI Conference on Artificial Intelligence*. Vol. 35. 12. 2021, pp. 10746–10753.
- [73] L. Grafakos. *Classical Fourier Analysis*. Vol. 2. Springer, 2008.
- [74] R. Piessens. “The Hankel transform.” *The Transforms and Applications Handbook 2.9* (2000).
- [75] F. Johansson et al. *mpmath: a Python library for arbitrary-precision floating-point arithmetic (version 0.18)*. <http://mpmath.org/>. 2013.
- [76] J. Long, E. Shelhamer, and T. Darrell. “Fully Convolutional Networks for Semantic Segmentation.” *CVPR*. 2015. arXiv: [1411.4038](https://arxiv.org/abs/1411.4038).
- [77] O. J. Hénaff, S. Koppula, J.-B. Alayrac, A. van den Oord, O. Vinyals, and J. Carreira. “Efficient Visual Pretraining with Contrastive Detection.” 2021. arXiv: [2103.10957](https://arxiv.org/abs/2103.10957).
- [78] K. He, G. Gkioxari, P. Dollár, and R. B. Girshick. “Mask R-CNN.” *ICCV*. 2017. arXiv: [1703.06870](https://arxiv.org/abs/1703.06870).
- [79] T.-Y. Lin, P. Dollár, R. B. Girshick, K. He, B. Hariharan, and S. J. Belongie. “Feature Pyramid Networks for Object Detection.” *CVPR*. 2017. arXiv: [1612.03144](https://arxiv.org/abs/1612.03144).

# Appendices

## A HSIC estimation in the self-supervised setting

Estimators of HSIC typically assume i.i.d. data, which is not the case for self-supervised learning – the positive examples are not independent. Here we show how to adapt our estimators to the self-supervision setting.

### A.1 Exact form of HSIC( $Z, Y$ )

Starting with HSIC( $Z, Y$ ), we assume that the “label”  $y$  is a one-hot encoding of the data point, and all  $N$  data points are sampled with the same probability  $1/N$ . With a one-hot encoding, any kernel that is a function of  $y_i^\top y_j$  or  $\|y_i - y_j\|$  (e.g. linear, Gaussian or IMQ) have the form

$$l(y_i, y_j) = \begin{cases} l_1 & y_i = y_j, \\ l_0 & \text{otherwise} \end{cases} \equiv \Delta l \mathbb{I}(y_i = y_j) + l_0 \quad (13)$$

for some  $\Delta l = l_1 - l_0$ .

**Theorem A.1.** *For a dataset with  $N$  original images sampled with probability  $1/N$ , and a kernel over image identities defined as in (13), HSIC( $Z, Y$ ) takes the form*

$$\text{HSIC}(Z, Y) = \frac{\Delta l}{N} \mathbb{E}_{Z, Z' \sim \text{pos}} [k(Z, Z')] - \frac{\Delta l}{N} \mathbb{E} [k(Z, Z')], \quad (14)$$

where  $Z, Z' \sim \text{pos}$  means  $p_{\text{pos}}(Z, Z') = \sum_i p(i)p(Z|i)p(Z'|i)$  for image probability  $p(i) = 1/N$ .

*Proof.* We compute HSIC (defined in (2)) term by term. Starting from the first, and denoting independent copies of  $Z, Y$  with  $Z', Y'$ ,

$$\begin{aligned} \mathbb{E} [k(Z, Z')l(Y, Y')] &= \Delta l \mathbb{E} [k(Z, Z')\mathbb{I}[Y = Y']] + l_0 \mathbb{E} [k(Z, Z')] \\ &= \Delta l \sum_{i=1}^N \sum_{j=1}^N \mathbb{E}_{Z|y_i, Z'|y_j} \left[ \frac{1}{N^2} k(Z, Z')\mathbb{I}[y_i = y_j] \right] + l_0 \mathbb{E} [k(Z, Z')] \\ &= \frac{\Delta l}{N} \sum_{i=1}^N \mathbb{E}_{Z|y_i, Z'|y_i} \left[ \frac{1}{N} k(Z, Z') \right] + l_0 \mathbb{E} [k(Z, Z')] \\ &= \frac{\Delta l}{N} \mathbb{E}_{Z, Z' \sim \text{pos}} [k(Z, Z')] + l_0 \mathbb{E} [k(Z, Z')], \end{aligned}$$

where  $\mathbb{E}_{Z, Z' \sim \text{pos}}$  is the expectation over positive examples (with  $Z$  and  $Z'$  are sampled independently conditioned on the “label”).

The second term, due to the independence between  $Z'$  and  $Y''$ , becomes

$$\mathbb{E} [k(Z, Z')l(Y, Y'')] = \mathbb{E}_{ZY} \mathbb{E}_{Z'} \left[ k(Z, Z') \left( \frac{\Delta l}{N} + l_0 \right) \right] = \left( \frac{\Delta l}{N} + l_0 \right) \mathbb{E} [k(Z, Z')].$$

And the last term becomes identical to the second one,

$$\mathbb{E} [k(Z, Z')] \mathbb{E} [l(Y, Y')] = \left( \frac{\Delta l}{N} + l_0 \right) \mathbb{E} [k(Z, Z')].$$

Therefore, we can write HSIC( $Z, Y$ ) as

$$\begin{aligned} \text{HSIC}(Z, Y) &= \mathbb{E} [k(Z, Z')l(Y, Y')] - 2 \mathbb{E} [k(Z, Z')l(Y, Y'')] + \mathbb{E} [k(Z, Z')] \mathbb{E} [l(Y, Y')] \\ &= \frac{\Delta l}{N} \mathbb{E}_{Z, Z' \sim \text{pos}} [k(Z, Z')] - \frac{\Delta l}{N} \mathbb{E} [k(Z, Z')], \end{aligned}$$

as the terms proportional to  $l_0$  cancel each other out.  $\square$

The final form of HSIC( $Z, Y$ ) shows that the  $Y$  kernel and dataset size come in only as pre-factors. To make the term independent of the dataset size (as long as it is finite), we can assume  $\Delta l = N$ , such that

$$\text{HSIC}(Z, Y) = \mathbb{E}_{Z, Z' \sim \text{pos}} [k(Z, Z')] - \mathbb{E} [k(Z, Z')].$$

## A.2 Estimator of HSIC(Z, Y)

**Theorem A.2.** *In the assumptions of Theorem A.1, additionally scale the Y kernel to have  $\Delta l = N$ , and the Z kernel to be  $k(z, z) = 1$ . Assume that the batch is sampled as follows:  $B < N$  original images are sampled without replacement, and for each image  $M$  positive examples are sampled independently (i.e., the standard sampling scheme in self-supervised learning). Then denoting each data point  $z_i^p$  for “label”  $i$  and positive example  $p$ ,*

$$\widehat{\text{HSIC}}(Z, Y) = \left( \frac{M}{M-1} + \frac{N-1}{N(B-1)} - \frac{M}{N(M-1)} \right) \frac{1}{BM^2} \sum_{ipl} k(z_i^p, z_i^l) \quad (15)$$

$$- \frac{B(N-1)}{(B-1)N} \frac{1}{B^2M^2} \sum_{ijpl} k(z_i^p, z_j^l) - \frac{N-1}{N(M-1)}. \quad (16)$$

is an unbiased estimator of (14).

While we assumed that  $k(z, z) = 1$  for simplicity, any change in the scaling would only affect the constant term (which is irrelevant for gradient-based learning). Recalling that  $|k(z, z')| \leq \max(k(z, z), k(z', z'))$ , we can then obtain a slightly biased estimator from Theorem A.2 by simply discarding small terms:

**Corollary A.2.1.** *If  $|k(z, z')| \leq 1$  for any  $z, z'$ , then*

$$\widehat{\text{HSIC}}(Z, Y) = \frac{1}{BM(M-1)} \sum_{ipl} k(z_i^p, z_i^l) - \frac{1}{B^2M^2} \sum_{ijpl} k(z_i^p, z_j^l) - \frac{1}{M-1} \quad (17)$$

has a  $O(1/B)$  bias.

*Proof of Theorem A.2.* To derive an unbiased estimator, we first compute expectations of two sums: one over all positives examples (same  $i$ ) and one over all data points.

Starting with the first,

$$\mathbb{E} \left[ \frac{1}{BM^2} \sum_{ipl} k(z_i^p, z_i^l) \right] = \mathbb{E} \left[ \frac{1}{BM^2} \sum_{ip, l \neq p} k(z_i^p, z_i^l) \right] + \mathbb{E} \left[ \frac{1}{BM^2} \sum_{ip} k(z_i^p, z_i^p) \right] \quad (18)$$

$$= \frac{M-1}{M} \mathbb{E}_{Z, Z' \sim \text{pos}} [k(Z, Z')] + \frac{1}{M}. \quad (19)$$

As for the second sum,

$$\mathbb{E} \left[ \frac{1}{B^2M^2} \sum_{ijpl} k(z_i^p, z_j^l) \right] = \mathbb{E} \left[ \frac{1}{B^2M^2} \sum_{i, j \neq i, pl} k(z_i^p, z_j^l) \right] + \mathbb{E} \left[ \frac{1}{B^2M^2} \sum_{ipl} k(z_i^p, z_i^l) \right].$$

The first term is tricky:  $\mathbb{E} [k(z_i^p, z_j^l)] \neq \mathbb{E} [k(Z, Z')]$  because we sample without replacement. But we know that  $p(y, y') = p(y)p(y'|y) = 1/(N(N-1))$ , therefore for  $i \neq j$

$$\mathbb{E} k(z_i^p, z_j^l) = \sum_{y, y' \neq y} \frac{1}{N(N-1)} \mathbb{E}_{Z|y, Z'|y'} k(Z, Z') \quad (20)$$

$$= \sum_{yy'} \frac{1}{N(N-1)} \mathbb{E}_{Z|y, Z'|y'} k(Z, Z') - \sum_y \frac{1}{N(N-1)} \mathbb{E}_{Z|y, Z'|y} k(Z, Z') \quad (21)$$

$$= \frac{N}{N-1} \mathbb{E} k(Z, Z') - \frac{1}{N-1} \mathbb{E}_{Z, Z' \sim \text{pos}} k(Z, Z'). \quad (22)$$

Using the expectations for  $ipl$  and  $ijpl$ ,

$$\mathbb{E} \frac{1}{B^2 M^2} \sum_{ijpl} k(z_i^p, z_j^l) = \mathbb{E} \frac{1}{B^2 M^2} \sum_{i,j \neq i, pl} k(z_i^p, z_j^l) + \mathbb{E} \frac{1}{B^2 M^2} \sum_{ipl} k(z_i^p, z_j^l) \quad (23)$$

$$= \frac{B-1}{B(N-1)} (N \mathbb{E} k(Z, Z') - \mathbb{E}_{Z, Z' \sim \text{pos}} k(Z, Z')) + \frac{M-1}{BM} \mathbb{E}_{Z, Z' \sim \text{pos}} k(Z, Z') + \frac{1}{BM} \quad (24)$$

$$= \frac{(B-1)N}{B(N-1)} \mathbb{E} k(Z, Z') - \frac{B-1}{B(N-1)} \mathbb{E}_{Z, Z' \sim \text{pos}} k(Z, Z') + \frac{M-1}{BM} \mathbb{E}_{Z, Z' \sim \text{pos}} k(Z, Z') + \frac{1}{BM} \quad (25)$$

$$= \frac{(B-1)N}{B(N-1)} \mathbb{E} k(Z, Z') + \frac{1}{B} \left( \frac{M-1}{M} - \frac{B-1}{N-1} \right) \mathbb{E}_{Z, Z' \sim \text{pos}} k(Z, Z') + \frac{1}{BM}. \quad (26)$$

Combining (18) and (23) shows that (15) is indeed an unbiased estimator.  $\square$

It's worth noting that the i.i.d. estimator (3) is flawed for  $\text{HSIC}(Z, Y)$  for two reasons: first, it misses the  $1/N$  scaling of  $\text{HSIC}(Z, Y)$  (however, it's easy to fix by rescaling); second, it misses the  $1/(M(M-1))$  correction for the  $ipl$  sum. As we typically have  $M = 2$ , the latter would result in a large bias for the (scaled) i.i.d. estimator.

### A.3 Estimator of $\text{HSIC}(Z, Z)$

Before discussing estimators of  $\text{HSIC}(Z, Z)$ , note that it takes the following form:

$$\text{HSIC}(Z, Z) = \mathbb{E} [k(Z, Z')^2] - 2\mathbb{E}_Z [\mathbb{E}_{Z'} [k(Z, Z')^2]] + (\mathbb{E} [k(Z, Z')])^2.$$

This is because  $X$  and  $Y$  in  $\text{HSIC}(X, Y)$  become the *same* random variable, so  $p(X, Y) = p_Z(X)\delta(X - Y)$  (see [28], Appendix A).

**Theorem A.3.** Assuming  $k(z, z') \leq 1$  for any  $z, z'$ , the i.i.d. HSIC estimator by Gretton et al. [26],

$$\widehat{\text{HSIC}}(Z, Z) = \frac{1}{(BM-1)^2} \text{Tr}(KHKH),$$

where  $H = I - \frac{1}{BM} \mathbf{1}\mathbf{1}^\top$ , has a  $O(1/B)$  bias for the self-supervised sampling scheme.

*Proof.* First, observe that

$$\text{Tr}(KHKH) = \text{Tr}(KK) - \frac{2}{BM} \mathbf{1}^\top KK \mathbf{1} + \frac{1}{B^2 M^2} (\mathbf{1}^\top K \mathbf{1})^2.$$

Starting with the first term, and using again the result of (20) for sampling without replacement,

$$\begin{aligned} \mathbb{E} [\text{Tr}(KK)] &= \mathbb{E} \left[ \sum_{ijpl} k(z_i^p, z_j^l)^2 \right] = \mathbb{E} \left[ \sum_{i,j \neq i, pl} k(z_i^p, z_j^l)^2 \right] + \mathbb{E} \left[ \sum_{ipl} k(z_i^p, z_j^l)^2 \right] \\ &= \frac{B(B-1)M^2}{N-1} (N \mathbb{E} k(Z, Z')^2 - \mathbb{E}_{Z, Z' \sim \text{pos}} k(Z, Z')^2) + \mathbb{E} \sum_{ipl} k(z_i^p, z_j^l)^2 \\ &= B^2 M^2 \mathbb{E} k(Z, Z')^2 + O(BM^2). \end{aligned}$$

Similarly, the expectation of the second term is

$$\begin{aligned} \mathbb{E} \mathbf{1}^\top KK \mathbf{1} &= \mathbb{E} \sum_{ijqpld} k(z_i^p, z_q^d) k(z_j^l, z_q^d) \\ &= \mathbb{E} \sum_{i,j \neq i, q \neq \{i,j\}, pld} k(z_i^p, z_q^d) k(z_j^l, z_q^d) + O(B^2 M^3). \end{aligned}$$

Here we again need to take sampling without replacement into account, and again it will produce a very small correction term. For  $i \neq j \neq q$ , repeating the calculation in (20),

$$\begin{aligned} \mathbb{E} k(z_i^p, z_j^l) k(z_i^p, z_q^d) &= \sum_{y, y' \neq y, y'' \neq \{y, y'\}} \frac{1}{N(N-1)(N-2)} \mathbb{E}_{Z|y, Z'|y', Z''|y''} k(Z, Z') k(Z, Z'') \\ &= \mathbb{E} k(Z, Z') k(Z, Z'') + O(1/N). \end{aligned}$$

As  $B < N$ , we obtain that

$$\mathbb{E} \mathbf{1}^\top K K \mathbf{1} = B(B-1)(B-2)M^3 \mathbb{E} k(Z, Z') k(Z, Z'') + O(B^2 M^3).$$

Finally, repeating the same argument for sampling without replacement,

$$\begin{aligned} \mathbb{E} (\mathbf{1}^\top K \mathbf{1})^2 &= \mathbb{E} \sum_{ijqrpldf} k(z_i^p, z_j^l) k(z_q^d, z_r^f) \\ &= \mathbb{E} \sum_{i, j \neq i, q \neq \{i, j\}, r \neq \{i, j, q\}, pldf} k(z_i^p, z_j^l) k(z_q^d, z_r^f) + O(B^3 M^4) \\ &= B(B-1)(B-2)(B-3)M^4 \mathbb{E} k(Z, Z') k(Z'', Z''') + O(B^3 M^4). \end{aligned}$$

Combining all terms together, and expressing  $B(B-1)$  (and similar) terms in big-O notation,

$$\begin{aligned} \mathbb{E} \frac{\text{Tr}(K H K H)}{(BM-1)^2} &= \mathbb{E} (k(Z, Z')^2 - 2k(Z, Z')k(Z, Z'') + k(Z, Z')k(Z'', Z''')) + O\left(\frac{1}{B}\right) \\ &= \mathbb{E} k(Z, Z')^2 - 2\mathbb{E}_Z (\mathbb{E}_{Z'} k(Z, Z'))^2 + (\mathbb{E} k(Z, Z'))^2 + O\left(\frac{1}{B}\right) \\ &= \text{HSIC}(Z, Z) + O\left(\frac{1}{B}\right). \end{aligned}$$

□

Essentially, having  $M$  positive examples for the batch size of  $BM$  changes the bias from  $O(1/(BM))$  (i.i.d. case) to  $O(1/B)$ . Finally, note that even if  $\widehat{\text{HSIC}}(Z, Z)$  is unbiased, its square root is not.

## B Theoretical properties of SSL-HSIC

### B.1 InfoNCE connection

To establish the connection with InfoNCE, define it in terms of expectations:

$$\mathcal{L}_{\text{InfoNCE}}(\theta) = \mathbb{E}_Z [\log \mathbb{E}_{Z'} [\exp(k(Z, Z'))]] - \mathbb{E}_{Z, Z' \sim \text{pos}} [k(Z, Z')]. \quad (27)$$

To clarify the reasoning in the main text, we can Taylor expand the exponent in (27) around  $\mu_1 \equiv \mathbb{E}_{Z'} [k(Z, Z')]$ . For  $k(Z, Z') \approx \mu_1$ ,

$$\begin{aligned} &\mathbb{E}_Z [\log \mathbb{E}_{Z'} [\exp(k(Z, Z'))]] \\ &\approx \mathbb{E}_Z [\mu_1] + \mathbb{E}_Z \left[ \log \mathbb{E}_{Z'} \left[ 1 + k(Z, Z') - \mu_1 + \frac{(k(Z, Z') - \mu_1)^2}{2} \right] \right] \\ &= \mathbb{E}_Z [\mu_1] + \mathbb{E}_Z \left[ \log \mathbb{E}_{Z'} \left[ 1 + \frac{(k(Z, Z') - \mu_1)^2}{2} \right] \right]. \end{aligned}$$

Now expanding  $\log(1+x)$  around zero,

$$\begin{aligned} \mathbb{E}_Z [\log \mathbb{E}_{Z'} [\exp(k(Z, Z'))]] &\approx \mathbb{E}_Z [\mu_1] + \mathbb{E}_Z \mathbb{E}_{Z'} \left[ \frac{(k(Z, Z') - \mu_1)^2}{2} \right] \\ &= \mathbb{E}_Z \mathbb{E}_{Z'} [k(Z, Z')] + \frac{1}{2} \mathbb{E}_Z [\text{Var}_{Z'} [k(Z, Z')]]. \end{aligned}$$



The approximate equality relates to expectations over higher order moments, which are dropped. The expression gives the required intuition behind the loss, however: when the variance in  $k(Z, Z')$  w.r.t.  $Z'$  is small, InfoNCE combines  $-\text{HSIC}(Z, Y)$  and a variance-based penalty. In general, we can always write (assuming  $\Delta l = N$  in  $\text{HSIC}(Z, Y)$  as before)

$$\mathcal{L}_{\text{InfoNCE}}(\theta) = -\text{HSIC}(Z, Y) + \mathbb{E}_Z [\log \mathbb{E}_{Z'} [\exp(k(Z, Z') - \mu_1)]] . \quad (28)$$

In the small variance regime, InfoNCE also bounds an HSIC-based loss. To show this, we will need a bound on  $\exp(x)$ :

**Lemma B.0.1.** For  $0 < \alpha \leq 1/4$  and  $x \geq -(1 + \sqrt{1 - 4\alpha}) / (2\alpha)$ ,

$$\exp(x) \geq 1 + x + \alpha x^2 . \quad (29)$$

*Proof.* The quadratic equation  $1 + x + \alpha x^2$  has two roots ( $x_1 \leq x_2$ ):

$$x_{1,2} = \frac{\pm\sqrt{1 - 4\alpha} - 1}{2\alpha} .$$

Both roots are real, as  $\alpha \leq 1/4$ . Between  $x_1$  and  $x_2$ , (29) holds trivially as the rhs is negative.

For  $x \geq -2$  and  $\alpha \leq 1/4$ ,

$$\exp(x) \geq 1 + x + \frac{x^2}{2!} + \frac{x^3}{3!} + \frac{x^4}{4!} + \frac{x^5}{5!} \geq 1 + x + \alpha x^2 .$$

The first bound always holds; the second follows from

$$\frac{x}{3!} + \frac{x^2}{4!} + \frac{x^3}{5!} \geq \alpha - \frac{1}{2} ,$$

as the lhs is monotonically increasing and equals  $-7/30$  at  $x = -2$ . The rhs is always smaller than  $-1/4 < -7/30$ . As  $x_2 \geq -2$  (due to  $\alpha \leq 1/4$ ), (29) holds for all  $x \geq x_1$ .  $\square$

We can now lower-bound InfoNCE:

**Theorem B.1.** Assuming that the kernel over  $Z$  is bounded as  $|k(z, z')| \leq k^{\max}$  for any  $z, z'$ , and the kernel over  $Y$  satisfies  $\Delta l = N$  (defined in (13)). Then for  $\gamma$  satisfying  $\min\{-2, -2k^{\max}\} = -(1 + \sqrt{1 - 4\gamma}) / (2\gamma)$ ,

$$-\text{HSIC}(Z, Y) + \gamma \text{HSIC}(Z, Z) \leq \mathcal{L}_{\text{InfoNCE}}(\theta) - \mathbb{E}_Z \frac{(\gamma \text{Var}_{Z'} [k(Z, Z')])^2}{1 + \gamma \text{Var}_{Z'} [k(Z, Z')]} .$$

*Proof.* As we assumed the kernel is bounded, for  $k(Z, Z') - \mu_1 \geq -2k^{\max}$  (almost surely; the factor of 2 comes from centering by  $\mu_1$ ). Now if we choose  $\gamma$  that satisfies  $\min\{-2, -2k^{\max}\} = -(1 + \sqrt{1 - 4\gamma}) / (2\gamma)$  (the minimum is to apply our bound even for  $k^{\max} < 1$ ), then (almost surely) by Lemma B.0.1,

$$\exp(k(Z, Z') - \mu_1) \geq 1 + k(Z, Z') - \mu_1 + \gamma (k(Z, Z') - \mu_1)^2 .$$

Therefore, we can take the expectation w.r.t.  $Z'$ , and obtain

$$\mathbb{E}_Z \log \mathbb{E}_{Z'} \exp(k(Z, Z') - \mu_1) \geq \mathbb{E}_Z \log (1 + \gamma \text{Var}_{Z'} [k(Z, Z')]) .$$

Now we can use that  $\log(1 + x) \geq x / (1 + x) = x - x^2 / (1 + x)$  for  $x > -1$ , resulting in

$$\mathbb{E}_Z \log \mathbb{E}_{Z'} \exp(k(Z, Z') - \mu_1) \geq \gamma \mathbb{E}_Z \text{Var}_{Z'} [k(Z, Z')] + \mathbb{E}_Z \frac{(\gamma \text{Var}_{Z'} [k(Z, Z')])^2}{1 + \gamma \text{Var}_{Z'} [k(Z, Z')]} .$$

Using (28), we obtain that

$$\begin{aligned} \mathcal{L}_{\text{InfoNCE}}(\theta) &= -\text{HSIC}(Z, Y) + \mathbb{E}_Z \log \mathbb{E}_{Z'} \exp(k(Z, Z') - \mu_1) \\ &\geq -\text{HSIC}(Z, Y) + \gamma \mathbb{E}_Z \text{Var}_{Z'} [k(Z, Z')] + \mathbb{E}_Z \frac{(\gamma \text{Var}_{Z'} [k(Z, Z')])^2}{1 + \gamma \text{Var}_{Z'} [k(Z, Z')]} . \end{aligned}$$

Finally, noting that by Cauchy-Schwarz

$$\begin{aligned} \text{HSIC}(Z, Z) &= \mathbb{E}_{Z, Z'} k(Z, Z')^2 - 2 \mathbb{E}_Z (\mathbb{E}_{Z'} k(Z, Z'))^2 + (\mathbb{E}_{Z, Z'} k(Z, Z'))^2 \\ &\leq \mathbb{E}_{Z, Z'} k(Z, Z')^2 - \mathbb{E}_Z (\mathbb{E}_{Z'} k(Z, Z'))^2 = \mathbb{E}_Z \text{Var}_{Z'} [k(Z, Z')] , \end{aligned}$$

we get the desired bound.  $\square$

Theorem B.1 works for any bounded kernel, because  $-(1 + \sqrt{1 - 4\gamma}) / (2\gamma)$  takes values in  $(\infty, -2]$  for  $\gamma \in (0, 1/4]$ . For inverse temperature-scaled cosine similarity kernel  $k(z, z') = z^\top z' / (\tau \|z\| \|z'\|)$ , we have  $k^{\max} = 1/\tau$ . For  $\tau = 0.1$  (used in SimCLR [19]), we get  $\gamma = 0.0475$ . For the Gaussian and the IMQ kernels,  $k(z, z') \geq -\mu_1 \geq -1$ , so we can replace  $\gamma$  with  $\frac{1}{3}$  due to the following inequality: for  $x \geq a$ ,

$$\exp(x) \geq 1 + x + \frac{x^2}{2} + \frac{x^3}{6} \geq 1 + x + \frac{a+3}{6} x^2 ,$$

where the first inequality is always true.

## B.2 MMD interpretation of HSIC(X,Y)

The special label structure of the self-supervised setting allows to understand  $\text{HSIC}(X, Y)$  in terms of the maximum mean discrepancy (MMD). Denoting labels as  $i$  and  $j$  and corresponding mean feature vectors (in the RKHS) as  $\mu_i$  and  $\mu_j$ ,

$$\text{MMD}^2(i, j) = \|\mu_i - \mu_j\|^2 = \langle \mu_i, \mu_i \rangle + \langle \mu_j, \mu_j \rangle - 2 \langle \mu_i, \mu_j \rangle .$$

Therefore, the average over all labels becomes

$$\begin{aligned} \frac{1}{N^2} \sum_{ij} \text{MMD}^2(i, j) &= \frac{2}{N} \sum_i \langle \mu_i, \mu_i \rangle - \frac{2}{N^2} \sum_{ij} \langle \mu_i, \mu_j \rangle \\ &= \frac{2}{N} \sum_i \langle \mu_i, \mu_i \rangle - \frac{2}{N^2} \left\langle \sum_i \mu_i, \sum_j \mu_j \right\rangle \\ &= 2 \mathbb{E}_i \mathbb{E}_{Z|i, Z'|i} \langle \phi(Z), \phi(Z') \rangle - 2 \langle \mathbb{E}_i \mathbb{E}_{Z|i} \phi(Z), \mathbb{E}_j \mathbb{E}_{Z'|j} \phi(Z') \rangle \\ &= 2 \mathbb{E}_{Z, Z' \sim \text{pos}} [k(Z, Z')] - 2 \mathbb{E}_Z \mathbb{E}_{Z'} [k(Z, Z')] , \end{aligned}$$

where the second last line uses that all labels have the same probability  $1/N$ , and the last line takes the expectation out of the dot product and uses  $k(Z, Z') = \langle \phi(Z), \phi(Z') \rangle$ .

Therefore,

$$\frac{1}{2N^2} \sum_{ij} \text{MMD}^2(i, j) = \frac{N}{\Delta l} \text{HSIC}(Z, Y) .$$

## B.3 Centered representation assumption for clustering

In Section 3.2, we make the assumption that the features are centered and argue that the assumption is valid for BYOL. Here we show empirical evidence of centered features. First, we train BYOL for 1000 epochs which reaches a top-1 accuracy of 74.5% similar to the reported result in [25]. Next, we extract feature representations (predictor and target projector outputs followed by re-normalization) under training data augmentations for a batch of 4096 images. One sample Z-test is carried out on the feature representations with  $H_0 : \mu = 0$  and  $H_1 : \mu \neq 0$ . The null hypothesis is accepted under threshold  $\alpha = 0.025$ .

## C Random Fourier Features (RFF)

### C.1 Basics of RFF

Random Fourier features were introduced by Rahimi and Recht [33] to reduce computational complexity of kernel methods. Briefly, for translation-invariant kernels  $k(z - z')$  that satisfy  $k(0) = 1$ ,

Bochner's theorem gives that

$$k(z - z') = \int p(\omega) e^{i\omega^\top(z-z')} d^n \omega = \mathbb{E}_\omega \left[ e^{i\omega^\top z} \left( e^{i\omega^\top z'} \right)^* \right],$$

where the probability distribution  $p(\omega)$  is the  $n$ -dimensional Fourier transform of  $k(z - z')$ .

As both the kernel and  $p(\omega)$  are real-valued, we only need the real parts of the exponent. Therefore, for  $b \sim \text{Uniform}[0, 2\pi]$ ,

$$k(z - z') = \mathbb{E}_{\omega, b} \left[ 2 \cos(\omega^\top z + b) \cos(\omega^\top z' + b) \right].$$

For  $N$  data points, we can draw  $D$   $\omega_d$  from  $p(\omega)$ , construct RFF for each points  $z_i$ , put them into matrix  $R \in \mathbb{R}^{N \times D}$ , and approximate the kernel matrix as

$$K \approx RR^\top, \quad R_{id} = \sqrt{\frac{2}{D}} \cos(\omega_d^\top z_i + b),$$

and  $\mathbb{E} RR^\top = K$ .

For the Gaussian kernel,  $k(z - z') = \exp(-\|z - z'\|^2/2)$ , we have  $p(\omega) = (2\pi)^{-D/2} \exp(-\|\omega\|^2/2)$  [33]. We are not aware of literature on RFF representation for the inverse multiquadratic (IMQ) kernel; we derive it below using standard methods.

## C.2 RFF for the IMQ kernel

**Theorem C.1.** *For the inverse multiquadratic (IMQ) kernel,*

$$k(z, z') \equiv k(z - z') = \frac{c}{\sqrt{c^2 + \|z - z'\|^2}},$$

the distribution of random Fourier features  $p(\omega)$  is proportional to the following (for  $s = \|\omega\|$ ),

$$p(\omega) \equiv \hat{h}(s) \propto \frac{K_{\frac{n-2}{2} + \frac{1}{2}}(cs)}{s^{\frac{n-2}{2} + \frac{1}{2}}} = \frac{K_{\frac{n-1}{2}}(cs)}{s^{\frac{n-1}{2}}}, \quad (30)$$

where  $K_\nu$  is the modified Bessel function (of the second kind) of order  $\nu$ .

*Proof.* To find the random Fourier features, we need to take the Fourier transform of this kernel,

$$\hat{k}(\omega) = \int e^{-i\omega^\top z} k(z) d^n z.$$

As the IMQ kernel is radially symmetric, meaning that  $k(z, z') = h(r)$  for  $r = \|z - z'\|$ , its Fourier transform can be written in terms of the Hankel transform [73, Section B.5] (with  $\|\omega\| = s$ )

$$\hat{k}(\omega) = \hat{h}(s) = \frac{(2\pi)^{n/2}}{s^{\frac{n-2}{2}}} H_{\frac{n-2}{2}} \left[ r^{\frac{n-2}{2}} h(r) \right] (s).$$

The Hankel transform of order  $\nu$  is defined as

$$H_\nu[g(t)](s) = \int_0^\infty J_\nu(st) g(t) t dt,$$

where  $J_\nu(s)$  is the Bessel function (of the first kind) of order  $\nu$ .

As  $h(r) = c/\sqrt{c^2 + r^2}$ ,

$$H_{\frac{n-2}{2}} \left[ r^{\frac{n-2}{2}} h(r) \right] (s) = c \frac{\sqrt{2} c^{\frac{n-2}{2} + 1/2}}{\sqrt{s} \Gamma(\frac{1}{2})} K_{\frac{n-2}{2} + \frac{1}{2}}(cs),$$

where  $K_\nu$  is a modified Bessel function (of the second kind) of order  $\nu$ .

Therefore, by using a table of Hankel transforms [74, Chapter 9, Table 9.2],

$$\hat{h}(s) \propto \frac{K_{\frac{n-2}{2} + \frac{1}{2}}(cs)}{s^{\frac{n-2}{2} + \frac{1}{2}}} = \frac{K_{\frac{n-1}{2}}(cs)}{s^{\frac{n-1}{2}}}.$$

□

### C.2.1 How to sample

To sample random vectors from (30), we can first sample their directions as uniformly distributed unit vectors  $d/\|d\|$ , and then their amplitudes  $s$  from  $\hat{h}(s)s^{n-1}$  (the multiplier comes from the change to spherical coordinates).

Sampling unit vectors is easy, as for  $d \sim \mathcal{N}(0, I)$ ,  $d/\|d\|$  is a uniformly distributed unit vector.

To sample the amplitudes, we numerically evaluate

$$\tilde{p}(s) = \hat{h}(s)s^{n-1} = K_{\frac{n-1}{2}}(cs)s^{\frac{n-1}{2}} \quad (31)$$

on a grid, normalize it to get a valid probability distribution, and sample from this approximation. As for large orders  $K_\nu$  attains very large numbers, we use mpmath [75], an arbitrary precision floating-point arithmetic library for Python. As we only need to sample  $\tilde{p}(s)$  once during training, this adds a negligible computational overhead.

Finally, note that for any IMQ bias  $c$ , we can sample  $s$  from (31) for  $c = 1$ , and then use  $\tilde{s} = s/c$  to rescale the amplitudes. This is because

$$P(s/c \leq x) = P(s \leq cx) = C \int_0^{cx} K_{\frac{n-1}{2}}(t)t^{\frac{n-1}{2}} dt = Cc^{\frac{n-1}{2}} \int_0^x K_{\frac{n-1}{2}}(ct)t^{\frac{n-1}{2}} cdt.$$

In practice, we evaluate  $\tilde{p}(s)$  for  $c = 1$  on a uniform grid over  $[10^{-12}, 100]$  with  $10^4$  points, and rescale for other  $c$  (for output dimensions of more than 128, we use a larger grid; see Appendix E).

### C.3 RFF for SSL-HSIC

To apply RFF to SSL-HSIC, we will discuss the  $\text{HSIC}(Z, Y)$  and the  $\text{HSIC}(Z, Z)$  terms separately. We will use the following notation:

$$k(z_i^p, z_j^l) \approx \sum_{d=1}^D r_d^{ip} r_d^{jl}$$

for  $D$ -dimensional RFF  $r^{ip}$  and  $r^{jl}$ .

Starting with the first term, we can re-write (17) as

$$\begin{aligned} \widehat{\text{HSIC}}(Z, Y)_{\text{RFF}} &= \frac{1}{BM(M-1)} \sum_{ipld} r_d^{ip} r_d^{il} - \frac{1}{B^2M^2} \sum_{ijpld} r_d^{ip} r_d^{jl} - \frac{1}{M-1} \\ &= \frac{1}{BM(M-1)} \sum_{id} \left( \sum_p r_d^{ip} \right)^2 - \frac{1}{B^2M^2} \sum_d \left( \sum_{ip} r_d^{ip} \right)^2 - \frac{1}{M-1}. \end{aligned}$$

The last term in the equation above is why we use RFF: instead of computing  $\sum_{ijpl}$  in  $O(B^2M^2)$  operations, we compute  $\sum_{ip}$  in  $O(BM)$  and then sum over  $d$ , resulting in  $O(BMD)$  operations (as we use large batches, typically  $BM > D$ ). As  $\text{HSIC}(Z, Y)$  is linear in  $k$ ,  $\mathbb{E}_{\omega, b} \widehat{\text{HSIC}}(Z, Y)_{\text{RFF}} = \widehat{\text{HSIC}}(Z, Y)$ .

To estimate  $\widehat{\text{HSIC}}(Z, Z)$ , we need to sample RFF twice. This is because

$$\widehat{\text{HSIC}}(Z, Z) = \frac{1}{(BM-1)^2} \text{Tr}(KHKH),$$

therefore we need the first  $K$  to be approximated by  $RR^\top$ , and the second – by an independently sampled  $\tilde{R}\tilde{R}^\top$ . This way, we will have  $\mathbb{E}_{\omega, b, \tilde{\omega}, \tilde{b}} \widehat{\text{HSIC}}(Z, Z)_{\text{RFF}} = \widehat{\text{HSIC}}(Z, Z)$ .

Therefore, we have (noting that  $HH = H$ )

$$\begin{aligned} \widehat{\text{HSIC}}(Z, Z)_{\text{RFF}} &= \frac{1}{(BM-1)^2} \text{Tr} \left( RR^\top H \tilde{R} \tilde{R}^\top H \right) = \frac{1}{(BM-1)^2} \|R^\top H \tilde{R}\|_F^2 \\ &= \frac{1}{(BM-1)^2} \|R^\top H H \tilde{R}\|_F^2 \\ &= \frac{1}{(BM-1)^2} \sum_{d_1, d_2} \left( \sum_{ip} \left( r_{d_1}^{ip} - \frac{1}{BM} \sum_{jl} r_{d_1}^{jl} \right) \left( r_{d_2}^{ip} - \frac{1}{BM} \sum_{jl} r_{d_2}^{jl} \right) \right)^2. \end{aligned}$$

To summarize the computational complexity of this approach, computing  $D$  random Fourier features for a  $Q$ -dimensional  $z$  takes  $O(DQ)$  operations (sampling  $D \times K$  Gaussian vector, normalizing it, sampling  $D$  amplitudes, computing  $\omega_d^\top z$   $D$  times), therefore  $O(BMDQ)$  for  $BM$  points. After that, computing  $\text{HSIC}(Z, Y)$  takes  $O(BMD)$  operations, and  $\text{HSIC}(Z, Z) - O(BMD^2)$  operations. The resulting complexity per batch is  $O(BMD(Q + D))$ . Note that we sample new features every batch.

In contrast, computing SSL-HSIC directly would cost  $O(Q)$  operations per entry of  $K$ , resulting in  $O((BM)^2Q)$  operations. Computing HSIC would then be quadratic in batch size, and the total complexity would stay  $O((BM)^2Q)$ .

In the majority of experiments,  $B = 4096$ ,  $M = 2$ ,  $Q = 128$  and  $D = 512$ , and the RFF approximation performs faster (with little change in accuracy; see Table 8b).

## D Experiment Details

### D.1 ImageNet Pretraining

#### D.1.1 Data augmentation

We follow the same data augmentation scheme as BYOL [25] with exactly the same parameters. For completeness, we list the augmentations applied and parameters used:

- random cropping: randomly sample an area of 8% to 100% of the original image with an aspect ratio logarithmically sampled from 3/4 to 4/3. The cropped image is resized to  $224 \times 224$  with bicubic interpolation;
- flip: optionally flip the image with a probability of 0.5;
- color jittering: adjusting brightness, contrast, saturation and hue in a random order with probabilities 0.8, 0.4, 0.4, 0.2 and 0.1 respectively;
- color dropping: optionally converting to grayscale with a probability of 0.2;
- Gaussian blurring: Gaussian kernel of size  $23 \times 23$  with a standard deviation uniformly sampled over  $[0.1, 2.0]$ ;
- solarization: optionally apply color transformation  $x \mapsto x \cdot \mathbf{1}_{x < 0.5} + (1 - x) \cdot \mathbf{1}_{x \geq 0.5}$  for pixels with values in  $[0, 1]$ . Solarization is only applied for the second view, with a probability of 0.2.



### D.1.2 Optimizing kernel parameters

Since we use radial basis function kernels, we can express the kernel  $k(s)$  in term of the distance  $s = \|z_i - z_j\|^2$ . The entropy of the kernel distance  $k_\sigma(s_{ij})$  can be expressed as follows:

$$\begin{aligned} H[k] &= - \int p(k) \log p(k) dk \\ &= - \int q(s) \log \left( q(s) \left| \frac{ds}{dk} \right| \right) ds \\ &= H[s] + \int q(s) \log \left| \frac{dk}{ds} \right| ds \\ &= \mathbb{E} [\log |k'_\sigma(s)|] + \text{const} \\ &\propto \mathbb{E} [\log |k'_\sigma(s)|^2] + \text{const}. \end{aligned}$$

We use the kernel distance entropy to automatically tune kernel parameters: for the kernel parameter  $\sigma$ , we update it to maximize  $\mathbb{E} [\log |k'_\sigma|^2]$  (for IMQ, we optimize the bias  $c$ ) at every batch. This procedure makes sure the kernel remains sensitive to data variations as representations move closer to each other.

## D.2 Evaluations

### D.2.1 ImageNet linear evaluation protocol

After pretraining with SSL-HSIC, we retain the encoder weights and train a linear layer on top of the frozen representation. The original ImageNet training set is split into a training set and a local validation set with 10000 data points. We train the linear layer on the training set. Spatial augmentations are applied during training, i.e., random crops with resizing to  $224 \times 224$  pixels, and random flips. For validation, images are resized to 256 pixels along the shorter side using bicubic resampling, after which a  $224 \times 224$  center crop is applied. We use SGD with Nesterov momentum and train over 90 epochs, with a batch size of 4096 and a momentum of 0.9. We sweep over learning rate and weight decay and choose the hyperparameter with top-1 accuracy on local validation set. With the best hyperparameter setting, we report the final performance on the original ImageNet validation set.

### D.2.2 ImageNet semi-supervised learning protocol

We use ImageNet 1% and 10% datasets as SimCLR [19]. During training, we initialize the weights to the pretrained weights, then fine-tune them on the ImageNet subsets. We use the same training procedure for augmentation and optimization as the linear evaluation protocol.

### D.2.3 Linear evaluation protocol for other classification datasets

We use the same dataset splits and follow the same procedure as BYOL [25] to evaluate classification performance on other datasets, i.e. 12 natural image datasets and Pascal VOC 2007. The frozen features are extracted from the frozen encoder. We learn a linear layer using logistic regression in `sklearn` with l2 penalty and LBFGS for optimization. We use the same local validation set as BYOL [25] and tune hyperparameter on this local validation set. Then, we train on the full training set using the chosen weight of the l2 penalty and report the final result on the test set.

### D.2.4 Fine-tuning protocol for other classification datasets

Using the same dataset splits described in Appendix D.2.3, we initialize the weights of the network to the pretrained weights and fine-tune on various classification tasks. The network is trained using SGD with Nesterov momentum for 20000 steps. The momentum parameter for the batch normalization statistics is set to  $\max(1 - 10/s, 0.9)$  where  $s$  is the number of steps per epoch. We sweep the weight decay and learning rate, and choose hyperparameters that give the best score on the local validation set. Then we use the selected weight decay and learning rate to train on the whole training set to report the test set performance.

## D.2.5 Transfer to semantic segmentation

In semantic segmentation, the goal is to classify each pixel. The head architecture is a fully-convolutional network (FCN)-based [76] architecture as [17, 25]. We train on the `train_aug2012` set and report results on `val2012`. Hyperparameters are selected on a 2119 images, which is the same held-out validation set as [25]. A standard per-pixel softmax cross-entropy loss is used to train the FCN. Training uses random scaling (by a ratio in [0.5, 2.0]), cropping (crop size 513), and horizontal flipping for data augmentation. Testing is performed on the [513, 513] central crop. We train for 30000 steps with a batch size of 16 and weight decay  $10^{-4}$ . We sweep the base learning rate with local validation set. We use the best learning rate to train on the whole training set and report on the test set. During training, the learning rate is multiplied by 0.1 at the 70th and 90th percentile of training. The final result is reported with the average of 5 seeds.

## D.2.6 Transfer to depth estimation

The network is trained to predict the depth map of a given scene. We use the same setup as BYOL [25] and report it here for completeness. The architecture is composed of a ResNet-50 backbone and a task head which takes the `conv5` features into 4 upsampling blocks with respective filter sizes 512, 256, 128, and 64. Reverse Huber loss function is used for training. The frames are down-sampled from [640, 480] by a factor 0.5 and center-cropped to size [304, 228]. Images are randomly flipped and color transformations are applied: greyscale with a probability of 0.3; brightness adjustment with a maximum difference of 0.1255; saturation with a saturation factor randomly picked in the interval [0.5, 1.5]; hue adjustment with a factor randomly picked in the interval [-0.2, 0.2]. We train for 7500 steps with batch size 256, weight decay 0.001, and learning rate 0.05.

## D.2.7 Transfer to object detection

We follow the same setup for evaluating COCO object detection tasks as in DetCon [77]. The architecture used is a Mask-RCNN [78] with feature pyramid networks [79]. During training, the images are randomly flipped and resized to  $(1024 \cdot s) \times (1024 \cdot s)$  where  $s \in [0.8, 1.25]$ . Then the resized image is cropped or padded to a  $1024 \times 1024$ . We fine-tune the model for 12 epochs ( $1 \times$  schedule [17]) with SGD with momentum with a learning rate of 0.3 and momentum 0.9. The learning rate increases linearly for the first 500 iterations and drops twice by a factor of 10, after 2/3 and 8/9 of the total training time. We apply a weight decay of  $4 \times 10^{-5}$  and train with a batch size of 64.

## E SSL-HSIC pseudo-code

```
import jax
import jax.numpy as jnp
import mpmath
import numpy as np

def ssl_hsic_loss(hiddens, kernel_param, num_rff_features, gamma, rng):
    """Compute SSL-HSIC loss."""
    hsic_yz = compute_hsic_yz(hiddens, num_rff_features, kernel_param, rng)
    hsic_zz = compute_hsic_zz(hiddens, num_rff_features, kernel_param, rng)
    return - hsic_yz + gamma * jnp.sqrt(hsic_zz)

def compute_hsic_yz(hiddens, num_rff_features, kernel_param, rng):
    """Compute RFF approximation of HSIC_YZ."""
    # B - batch size; M - Number of transformations.
    B = hiddens[0].shape[0]
    M = len(hiddens)

    rff_hiddens = jnp.zeros((B, num_rff_features))
    mean = jnp.zeros((1, num_rff_features))
    for hidden in hiddens:
        rff_features = imq_rff_features(hidden, num_rff_features, kernel_param, rng)
        rff_hiddens += rff_features
        mean += rff_features.sum(0, keepdims=True)
    return (rff_hiddens ** 2).sum() / (B * K * (K - 1)) - (mean ** 2).sum() / (B * M) ** 2

def compute_hsic_zz(hiddens, num_rff_features, kernel_param, rng):
    """Compute RFF approximation of HSIC_ZZ."""
    rng_1, rng_2 = jax.random.split(rng, num=2)
    B = hiddens[0].shape[0]
```

```

M = len(hiddens)

z1_rffs = []
z2_rffs = []
center_z1 = jnp.zeros((1, num_rff_features))
center_z2 = jnp.zeros((1, num_rff_features))
for hidden in hiddens:
    z1_rff = imq_rff_features(hidden, num_rff_features, kernel_param, rng_1)
    z2_rff = imq_rff_features(hidden, num_rff_features, kernel_param, rng_2)
    z1_rffs.append(z1_rff)
    center_z1 += z1_rff.mean(0, keepdims=True)
    z2_rffs.append(z2_rff)
    center_z2 += z2_rff.mean(0, keepdims=True)
center_z1 /= M
center_z2 /= M

z = jnp.zeros(shape=(num_rff_features, num_rff_features), dtype=jnp.float32)
for z1_rff, z2_rff in zip(z1_rffs, z2_rffs):
    z += jnp.einsum('ni,nj->ij', z1_rff - center_z1, z2_rff - center_z2)
return (z ** 2).sum() / (B * M - 1) ** 2

def imq_rff_features(hidden, num_rff_features, kernel_param, rng):
    """Random Fourier features of IMQ kernel."""
    d = hidden.shape[-1]
    rng1, rng2 = jax.random.split(rng)
    amp, amp_probs = amplitude_frequency_and_probs(d)
    amplitudes = jax.random.choice(rng1, amp, shape=[num_rff_features, 1], p=amp_probs)
    directions = jax.random.normal(rng2, shape=(num_rff_features, d))
    b = jax.random.uniform(rng2, shape=(1, num_features)) * 2 * jnp.pi
    w = directions / jnp.linalg.norm(directions, axis=-1, keepdims=True) * amplitudes
    z = jnp.sqrt(2 / num_rff_features) * jnp.cos(jnp.matmul(hidden / kernel_param, w.T) + b)
    return z

def amplitude_frequency_and_probs(d):
    """Returns frequencies and probabilities of amplitude for RFF of IMQ kernel."""
    # Heuristics for increasing the upper limit with the feature dimension.
    if d >= 4096:
        upper = 200
    elif d >= 2048:
        upper = 150
    elif d >= 1024:
        upper = 120
    else:
        upper = 100
    x = np.linspace(1e-12, upper, 10000)
    p = compute_prob(d, x)
    return x, p

def compute_prob(d, x_range):
    """Returns probabilities associated with the frequencies."""
    prob = list()
    for x in x_range:
        prob.append(mpmath.besselk((d - 1) / 2, x) * mpmath.power(x, (d - 1) / 2))
    normalizer = prob[0]
    for x in prob[1:]:
        normalizer += x
    normalized_prob = []
    for x in prob:
        normalized_prob.append(float(x / normalizer))
    return np.array(normalized_prob)

```